Journal of Ocean Engineering and Science xxx (xxxx) xxx

Contents lists available at ScienceDirect

Journal of Ocean Engineering and Science

journal homepage: www.elsevier.com/locate/joes

Original Article

Coupled aero-hydro-servo-elastic analysis of 10MW TLB floating offshore wind turbine

Iman Ramzanpoor[a], Martin Nuernberg[b], Longbin Tao[a,*]

[a] Department of Naval Archicture, Ocean & Marine Engineering, University of Strathclyde, Glasgow, G4 0LZ, UK
[b] Newcastle Marine Services Ltd., Newcastle upon Tyne, NE12 9SZ, UK

ARTICLE INFO

Article history:
Received 20 October 2022
Revised 27 February 2023
Accepted 27 February 2023
Available online xxx

Keywords:
Floating wind turbines
Tension leg buoy
Aerodynamics & hydrodynamics
Taut Mooring

ABSTRACT

This paper presents a fully coupled aero-hydro-servo elastic analysis of a 10MW offshore wind turbine supported by a tension leg buoy (TLB) platform, with a taut mooring system. The study investigates the TLB's dynamic response characteristics under the northern North Sea environmental conditions with water depths of 110 metres, comparing the performance of steel, polyester, and nylon mooring line configurations. Innovating floating wind turbines requires a cost-effective system that achieves reliable performance in operational and survival conditions. The innovative system should compete with other existing FOWT types and fixed-bottom offshore wind turbines in terms of LCOE. The dynamic responses of the relatively less complex TLB platform in terms of construction and installation showed small motion and accelerations for all available mooring materials from the current supply chain, enabling the wind turbine to be installed without significant modifications to their control systems. The mooring materials' elasticity is essential in the system achieving motion response.

1. Introduction

Over the last two decades, the demand for renewable energy, including offshore wind, has been increasing rapidly because of the drive to reduce CO2 emission. This demand is expected to continue accelerating over the coming years even whilst fossil fuels remain the most significant provider of the world's energy in the decades ahead [1]. In the UK specifically, the Committee on Climate Change has recommended a new emissions target, such that all greenhouse gases (GHGs) that contribute to climate change must be reduced substantially to meet the Paris temperature goal, to achieve net-zero GHG emissions by 2050. This means that the UK became the first major economy in the world to pass laws to end its contribution to global warming by 2050 [2]. Wind energy has been one of the fastest-growing renewable energy technologies in recent years, and it attracts further attention due to ambitious targets for renewable energy electricity production in offshore areas [3]. However, this growth can only be achieved if wind turbines are deployed into deep-water areas, where vast wind energy resources with increased energy density are available. Floating offshore wind turbines (FOWT) can be the solution to this problem, allowing more robust wind resources in far offshore deep-water locations to be harnessed.

There is significant potential and desire for offshore wind energy market growth in the UK due to the existence of appropriate locations with extensive wind resources beyond 50 m water depth suitable for FOWT deployment [4–6]. It is estimated that about 70% of global wind energy resources are located in areas offshore with water depths of 50 m or more [7]. The potential for electricity generation from FOWT in the UK is significant, due to over half of the North Sea having water depths between 50 m to 220 m, and therefore being appropriate for FOWT deployment [8]. Based on predictions by EWEA, most of the developments up to 2030 will focus in the North Sea and Baltic Sea, with the average water depth and distance to shore for offshore wind farms increasing up to 215 m and 200 km, respectively [7].

According to the development history of wind turbines, the rated power of the turbines has risen from 50 kW with a hub height of about 25 m, to more than 10MW with a hub height of 120 m [9]. This is because larger rotors and blades can cover a wider area, increasing the turbine's capacity to produce higher total potential as the blades rise higher into the atmosphere, the

* Corresponding author.
E-mail address: longbin.tao@strath.ac.uk (L. Tao).

https://doi.org/10.1016/j.joes.2023.02.001

wind blows more steadily, and the capacity factor of the turbine increases.

Spar Buoy, Semi-Submersible and tension leg platforms (TLP) are the current leading technology types for floating offshore wind power, and have been adapted from the offshore oil and gas industry [10]. Each of them has its own characteristics, and can be categorised based on the implemented primary mechanism to fulfil the static stability requirements [11]. The current key challenge in the FOWT industry and research is designing economically efficient floating systems that can compete with other existing FOWT types and fixed-bottom offshore wind turbines in terms of LCOE [12]. By comparing the current leading technology types for floating offshore wind power, it can be observed that current levelized cost of energy (LCOE) values are strongly dependant on the type of support structure design, mooring line design, water depth and distance from shore [8]. Hence, to reduce the cost, the design and construction complexity of the platform needs to be reduced, whilst also introducing an optimum solution for the mooring system. The critical point for developing concepts within each form of technology is to consider at an early stage in the design process that the design capabilities are as flexible as possible, thus facilitating the platforms adaptation to a range of installation sites [13].

The tension leg buoy (TLB) platform described in this project is developed based on the concept proposed by Sclavonous [14] and later by Myhr [15]. The TLB concept has several design advantages compared to other floating concepts, first of which is that it is a simple design, with the possibility of a low draft, therefore reducing material consumption. Secondly, the motion response characteristics are lower than those of other floating foundation concepts due to the taut mooring lines. Thirdly, the close anchor spacing allows for potential anchor sharing between adjacent turbines in a closely spaced array. However, the technological aspect of TLB concepts is still facing a challenge due to the relatively high mooring line and anchor loads [16]. As a result, the key focus in recent years has been to investigate ways to reduce these loads. If successful, such a floating system will most likely be cost-efficient at or beyond 50 m water depth. The TLB design can be constructed and to be assembled in the port then towed out to the deployment location and then by de-ballasting, the platform hooks into the mooring lines. Therefore, the expenditure on the support vessel will reduce.

According to increased rated power over the decade [9], appropriate locations with suitable depth deploying FOWTs [7], and the advantages of TLB FOWT over those of other floating foundation concepts, the present study considers a 10MW TLB FOWT to deploy in Northern North Sea with 110 m water depth.

This study applies frequency domain and time domain analyses to a 10MW TLB FOWT. Aero-hydro-elastic analysis will be carried within the time domain coupled analysis of the complete turbine-structure-mooring system. The second-order wave forces and added mass is computed based on potential theory in the hydrodynamic analysis code WADAM [17], which is integrated through HydroD into the DNVGL SESAM software package [18]. The coupled motion response of the TLB system under the defined environmental conditions are simulated using SIMO/RIFLEX in SESAM's SIMA program [19,20], allowing for excitation force, motion response and mooring line response calculations, while considering full aerodynamic effects from the rotating turbine on the system. The simulations are conducted for three hours duration, studying the performance of the complete system in design and extreme conditions. Specifically, motion response of the platform, nacelle movements, accelerations and vibration, tensions on mooring lines, and system stability with under damaged mooring system are analysed.

Floating wind turbine technology requires continued innovation to achieve reliable performance and reduced investment costs for mass production. As pioneering design concepts are currently at the initial stages of development, innovation and knowledge through research are essential to progress in the field. System design needs to develop tools to predict loads and optimise for specific conditions, including operational and survival conditions. Measurement campaigns are required to improve model tools in the field and controlled test facilities.

An innovative approach presented in this paper lies in the use of coupled, high fidelity, models to explore the impact that deploying synthetic mooring lines and innovative material mooring components can be a solution for deploying large scale floating offshore wind turbines in relatively shallow waters. The analyse aims to show that the designed TLB platform with mooring system designed would be capable of supporting the static and dynamic operation and survival requirements of a 10MW FOWT with a control system developed specifically for land-based wind turbines. By integrating the potential for novel anchor sharing applications into the mooring design stage, the methodology ensures that motion, loads and distances between turbines allow industry standard spacing between adjacent turbines to limit the effects on performance when operating in wakes of the upstream turbines. Investigating the feasibility of utilising polyester or nylon based mooring lines at this scale provides the requirements in terms of elasticity, minimum loads and safety factors to the developers or mooring materials for the FOWT industry.

The paper is structured as follows; Section 2 provides the environmental conditions and site location, whilst Section 3 describes the configuration of the 10MW TLB FOWT with mooring system. Section 4 introduces the methodology and numerical methods that are used for fully coupled aero-hydro-elastic analysis, before Section 5 where detailed results and discussions on the findings presents. Conclusions are presented in Section 6.

2. Environmental condition

Wind turbines are exposed structures subject to various external effects and operating in medium to high wind speeds is a functional requirement. Conditions such as steady and turbulence wind also form a significant source for the loading of wind turbines.

A typical example of a far-offshore FOWT location is Buchan Deep, 25 km offshore of Peterhead, where Statoil installed a 30MW wind turbine farm on floating structures (Hywind Spar) to harness Scottish wind resources. The water depth of these locations was between 95 m to 120 m [21]. The northern North Sea was chosen in an early assessment, based on the excellent wind resources, and representative water depth, and distance to shore. The present study considers a location off the Scottish Coast, with water depth 110 m, comparable to that of the Hywind Demonstrator Farm.

2.1. Environmental design load cases

The load analysis involves verifying the system's integrity by considering a series of design load cases (DLCs) to help determine the extreme and accidental loads expected over the system's lifetime. The design load cases introduced by DNVGL [22–24] cover essential design- situations such as normal operation conditions and parked or idling state. These include appropriate normal and extreme external conditions and fault scenarios. It is noted that there is no need for this preliminary load analysis to apply all the load cases prescribed by the design standard [25]. This study aims to utilize the ultimate load type during survival and operational conditions and investigates accidental loads to assess whether the system will survive under the failure of a set of mooring lines.

Table 1
Combined Environmental Load Cases [23,24].

Event	DLC	Wind	Wave	Current
Power Production	**1.1**	NTM $V_{in}<U_{10,\ Hub}<V_{out}$	NSS $H_s= H_S$ at $U_{10,\ Hub}$	Wind Generated Current
	1.6a	NTM $V_{in}<U_{10,\ Hub}<V_{out}$	SSS $H_s= H_{S,50yr}$	Wind Generated Current
Parked	**6.1a**	EWM Turbulent Wind, $U_{10,Hub}$	ESS $H_s= H_{S,50yr}$	V_{50yr}
	6.2b	EWM Steady Wind, $U_{10,\ Hub}$	ESS $H_s= H_{S,50yr}$	V_{50yr}
Parked with Fault	**7.1a**	EWM Turbulent Wind, $U_{10,\ Hub}$	ESS $H_s= H_{S,1yr}$	V_{1yr}
	7.1b	EWM Steady Wind, $U_{10,\ Hub}=1.4U_{10,1yr}$	RWH $H_s=\Psi\ H_{S,1yr}$	V_{1yr}

For the parked event, the influence of wind turbulence intensity on TLB FOWT motion responses and tension load in mooring lines is evaluated, as this is varied between a wind model with and without turbulence for the two design load cases. According to IEC-61,400–1 & 3 [23,26], wind turbine generator system (WTGS) classes are defined in terms of wind speed and turbulence parameters. The extreme wind conditions are used to determine extreme wind loads on WTGS. These conditions include peak wind speeds due to storms and rapid changes in wind speed and direction. These extreme conditions include the potential effects of wind turbulence so that only the deterministic effects need to be considered in the design calculations. By having the characteristic value of the turbulence intensity at 15 m/s, $I_{15} = 0.18$, designated the category for higher turbulence characteristics is considered for DLC6.1a. These wind models are coded in TurbSim.

According to DNVGL-OS-E301 [27], ALS is an accidental limit state to ensure that the mooring system has adequate capacity to withstand the failure of one mooring line. Based on DNVGL-ST-0119 [28] Section 7.4.3, the load pattern of an anchor shared by two or more mooring lines may change significantly, thus one line at each mooring cluster sets to be broken for ALS. Therefore, one mooring line at each cluster is assumed to be disconnected after 100 s of the simulation to represent the ALS scenario for parked with fault event.

Therefore, six combined environmental load cases are defined for this study shown in Table 1, based on DNVGL-ST-0437 [24]. The directionality of the environmental loads considered for this study is collinear.

3. 10MW tlb fowt

The end goal is to have an alternative system with reduced costs and other complexities in terms of construction, installation, and transportation compared to the existing types of FOWT. It is also essential to have a FOWT design with limited motion responses allow for ease of adoption of land-based wind turbines without the need to re-develop control systems. It should be considering at an early stage in the design process that the design be as flexible as possible to facilitate adaption for different sites.

The less complex TLB design is aiming to provide a cost effective, flexible alternative platform solution for large scale FOWT development around the UK. By having a simplify the construction and installation processes, full designs can be towed and connected to the mooring before being de-ballasted to achieve the required pretension.

The first design iteration was performed by gradually increasing the platform excess buoyancy and mooring stiffness through varying the platform dimensions and mooring line radius to ensure the coupled system's proper motion and mooring performance in operational and survival conditions. In the second stage of design iterations, the number of mooring lines was gradually increased to satisfy the ULS and ALS (Fig. 1). Combining a new approach of determining the stiffness matrix for the taut mooring system with a detailed frequency and time domain analysis to investigate the dynamic performance of the TLB.

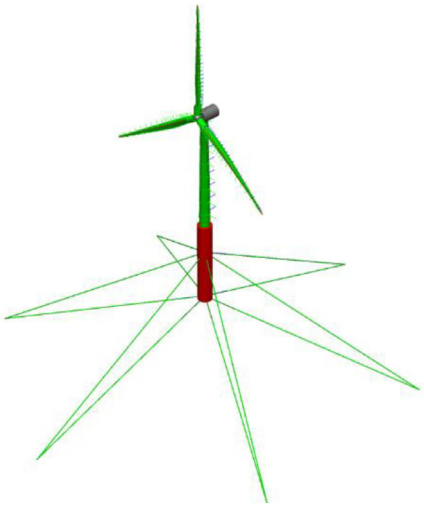

Fig. 1. Floating System Overview.

3.1. Wind turbine

The DTU 10MW RWT wind turbine designed and developed by Technical University of Denmark [29] is employed for analysis in this study. This development is originally designed for operations onshore, and so the tower characteristics need be modified for application on the floating platform; shortening the total tower length to fit between the top of the floater (at 20 m above sea level) to the underside of the nacelle (at about 119 m above sea level). This can be achieved either by modifying the ratio of the tower masses or the height ratio [30]. The total tower length was shortened by the height ratio to reduce the overturning bending moments.

The present simulation also ignores the blade flexibility which could influence the system dynamics, particularly the tower elastic motion response when the rotor experiences severe aerodynamic loads at which interaction between the blade and tower elastic motions can be evident.

3.2. TLB platform

The first application of the TLB concept for use as a FOWT was presented in 2005 as the MIT Double Taut Leg [34,35]. The floating support platform TLB is composed of a cylindrical shape to support the tower and the wind turbine. The TLB presented in this paper is based on the 5MW TLB system designed by Anders Myhr [15] but scaled to support the 10MW DTU system. The most significant consideration in scaling the floating platform from previous studies (Myhr 2016) is ensuring its excess buoyancy levels remain sufficient for the system to achieve stability. Fig. 2 and Table 2 illustrate the configuration and characteristics of the platform.

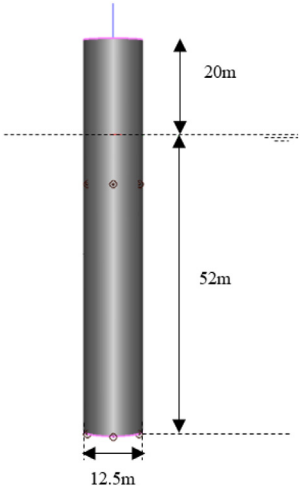

Fig. 2. TLB Support Platform.

Table 2
Support Platform Specification.

TLB Platform	
Draft	52m
Diameter SWL	12.5m
Diameter Bottom	12.5m
Mass	791.0t
COG	40.95m
COB	−26m
Pre-Tension	906.8t

Note: water line is used as the reference point.

3.3. Mooring system

Similar to Trolle and Hornbak [31], a taut mooring system is designed for a TLB FOWT. This design uses fibre ropes which are tensioned in a taut mooring configuration. Taut mooring is commonly used in deep water, where it becomes both a cheaper and lighter solution while providing a smaller footprint than catenary mooring. The innovative taut mooring system has advantageous over the catenary mooring line where long section of lines must be placed on the seabed in the catenary mooring system, whilst the taut mooring system doesn't touch the seabed. Another advantage of small motion responses of the TLB with taut mooring system is that more platforms can be deployed in the limited wind farm area, especially due to the surge motion response from taut mooring system being considerably less than the platforms with catenary mooring and TLP type platforms. Two set of clusters of mooring system designed. The first mooring cluster, the mooring lines are attached to the TLB 10 m below the SWL and the second cluster of mooring lines attached to the bottom of floater. By attaching the mooring lines to 10 m below SWL, having sufficient draft which allows any vessel to approach the platform for service & maintenance operations.

The analysis assumes the line material and cross section are uniform and the line structural elongation is governed by Hooke's law. Quasi-static cable models developed to determine the mooring lines tensions which ignored the cable inertia forces, external fluid loads such as drag and added mass forces, and cable seabed interaction forces. Quasi–static cable models are often used in dynamic simulations of offshore structures due to the ease of implementation.

As in HydroD there is no mooring line presents, hence, the representation of mooring system in the hydrostatic evaluation includes the hydrostatic stiffness matrix calculated for each mooring material as follows to account for the taut mooring system.

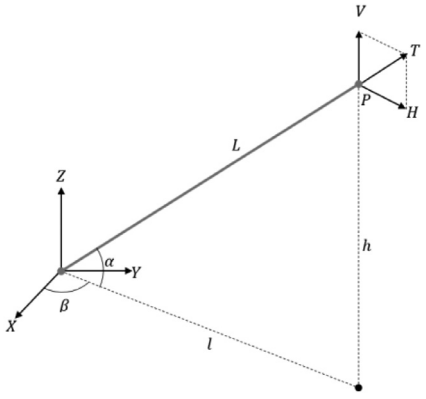

Fig. 3. Taut Line.

By considering a single mooring line suspended at P, shows in Fig. 3, Eq. (1) shows the expression of the stiffness matrix of the cable in the plane of the cable profile [32,33].

$$K^P = \begin{bmatrix} K^P_{11} & K^P_{12} \\ K^P_{21} & K^P_{22} \end{bmatrix} = \begin{bmatrix} \frac{\partial H}{\partial l} & \frac{\partial H}{\partial h} \\ \frac{\partial V}{\partial l} & \frac{\partial V}{\partial h} \end{bmatrix} \tag{1}$$

When the line is taut and no sag exists i.e., $\frac{H}{V} \approx \frac{l}{h}$, it can be modelled accurately as a massless linear spring to simplify the computations. The stiffness of the tether along its chord (L) can be assumed equal to $K_l = \frac{EA}{L_o}$, as shows in Fig. 3.

The massless spring assumption dramatically simplifies the analysis. This simplified analytical approach can provide an accurate approximation of the stiffness for taut mooring system [34]. Consider the cable shown in Fig. 3 of unstretched length L_o, stretched length (chord length), $L = \sqrt{l^2 + h^2}$ Its configuration is defined by angles β and α. When the cable is stretched by ΔL, the associated variation of tension is $\Delta T = K_l \Delta L$. The cable tension is $T = K_l\,(L - L_o)$. The expressions for $H,\ V,\ l$, and h can be then written as

$$H = T\cos\,\alpha,\ V = T\sin\,\alpha,\ l = L\cos\,\alpha,\ h = L\sin\,\alpha \tag{2}$$

In contrast to the previous two cases, the elements of K^P can be directly derived as

$$\begin{aligned}
\frac{\partial H}{\partial l} &= \frac{\partial (T\cos\,\alpha)}{\partial l} = \cos\,\alpha \frac{\partial T}{\partial L}\frac{\partial L}{\partial l} + T\left(-\sin\alpha \frac{\partial \alpha}{\partial l}\right) \\
\frac{\partial H}{\partial h} &= \frac{\partial (T\cos\,\alpha)}{\partial h} = \cos\,\alpha \frac{\partial T}{\partial L}\frac{\partial L}{\partial h} + T\left(-\sin\alpha \frac{\partial \alpha}{\partial h}\right) \\
\frac{\partial V}{\partial l} &= \frac{\partial (T\sin\,\alpha)}{\partial l} = \sin\,\alpha \frac{\partial T}{\partial L}\frac{\partial L}{\partial l} + T\cos\alpha \frac{\partial \alpha}{\partial l} \\
\frac{\partial V}{\partial h} &= \frac{\partial (T\sin\,\alpha)}{\partial l} = \sin\,\alpha \frac{\partial T}{\partial L}\frac{\partial L}{\partial h} + T\cos\alpha \frac{\partial \alpha}{\partial h}
\end{aligned} \tag{3}$$

It is obvious that when the cable is taut, $T = f(L)$ such that $\frac{\partial T}{\partial L} = \frac{dT}{dL} = K_l$.

From kinematics we can evaluate the partial derivatives of L, with respect to l, and h and the final form of the elements of the cable plane stiffness matrix K^P can be obtained as

$$\begin{aligned}
\frac{\partial H}{\partial l} &= \cos^2\alpha K_l + \frac{T}{L}\sin^2\alpha \\
\frac{\partial V}{\partial h} &= \sin^2\alpha K_l + \frac{T}{L}\cos^2\alpha \\
\frac{\partial H}{\partial h} &= \frac{\partial V}{\partial l} = \cos\alpha \sin\,\alpha\left(K_l - \frac{T}{L}\right)
\end{aligned} \tag{4}$$

The mooring stiffness matrix of the entire mooring system at equilibrium is symmetric, can be then expressed as

$$K_m = \begin{bmatrix} K_{11} & 0 & 0 & 0 & K_{15} & 0 \\ 0 & K_{22} & 0 & K_{24} & 0 & 0 \\ 0 & 0 & K_{33} & 0 & 0 & 0 \\ 0 & K_{42} & 0 & K_{44} & 0 & 0 \\ K_{51} & 0 & 0 & 0 & K_{55} & 0 \\ 0 & 0 & 0 & 0 & 0 & K_{66} \end{bmatrix} \tag{5}$$

The stiffness matrix of a symmetric taut mooring system can be obtained by Eq. (6) to (13). The restoring matrix is calculated for one cluster and the complete stiffness matrix is composed of multiple lines calculated by adding the stiffness matrices of the individual lines following the procedure presented in [34].

$$K_{11} = \frac{n}{2}\left[\frac{T}{L}\left(1+\sin^2\alpha\right) + K_l \cos^2\alpha\right] \tag{6}$$

$$K_{15} = -n\left[\frac{T}{2L}\left(D + D\sin^2\alpha\right) + R\ sin\ \alpha\ cos\ \alpha\right) + \frac{K_l}{2}\left(D cos^2\alpha - R\ sin\ \alpha\ cos\ \alpha\right] \tag{7}$$

$$K_{22} = K_{11},\ \ K_{24} = -K_{15} \tag{8}$$

$$K_{33} = n\left[\frac{T}{L}\cos^2\alpha + K_l \sin^2\alpha\right] \tag{9}$$

$$K_{44} = n\left\{T\ \left(D\sin\alpha + \frac{R}{2}\ \cos\alpha\right) + \frac{T}{2L}\left[(R\cos\alpha + D\sin\alpha)^2 + D^2\right] + \frac{K_l}{2}(D\cos\alpha - R\sin\alpha)^2\right\} \tag{10}$$

$$K_{42} = K_{24} \tag{11}$$

$$K_{51} = K_{15},\ \ K_{55} = K_{44} \tag{12}$$

$$K_{66} = n\frac{TR}{L}(R + L\cos\alpha) \tag{13}$$

In the preceding equations, n is the number of mooring lines, T is tension per mooring line, α is the angle of mooring line attached to fairlead, L is the mooring line length, $K_l = \frac{EA}{L}$ is the stiffness of the tether along its chord, D is the fairlead distance to SWL, and R is the floater radius. The total hydrostatic stiffness matrix K_m calculated presents in Eq. (14) for the system moored with steel mooring rope. It should be noted that the K_m is different for each mooring material, due to K_l.

$$K_m = \begin{bmatrix} 2.59E+10 & 0 & 0 & 0 & -8.05E+11 & 0 \\ 0 & 2.59E+10 & 0 & 8.05E+11 & 0 & 0 \\ 0 & 0 & 1.07E+10 & 0 & 0 & 0 \\ 0 & 8.05E+11 & 0 & 9.65E+14 & 0 & 0 \\ -8.05E+11 & 0 & 0 & 0 & 9.65E+14 & 0 \\ 0 & 0 & 0 & 0 & 0 & 1.13E+09 \end{bmatrix} \tag{14}$$

The influence of the VIV which can be considerable when the substructure is subject to steady current or combined current and wave loads is also neglected. All simplified assumptions could reduce the accuracy of the predicted hydrodynamic loads exerted on the platform and mooring lines particularly in low and moderate fluid speeds which may affect the resulting system response.

The mooring system configuration and principal properties are present in Table 3 and Fig. 4 and Fig. 5.

Table 3
Mooring System Principal Properties.

Taut Mooring system Characteristics	
No. of Lines	2 sets of 6 lines
Angle between Lines	60°
Radius Plat. CL to Anchor	180m
Fairlead below SWL	−10 m & −52m
Angle of attached at top Fairlead	29.92 °
Angle of attached at bottom Fairlead	18.46 °

Table 4
Mooring Material Specifications.

	Diameter (mm)	$W_{in\ Air}$ (kg/m)	$W_{in\ Water}$ (kg/m)	MBF (tons)
Steel	240	221.6	176.6	3000
Polyester	310	64	16.5	2900
Nylon	320	47.8	4.82	2247

The mooring system is defined by the anchor radius (R_C), water depth (d_w) and depth to both attachment points of the fairleads for upper (d_u) and lower (d_L) mooring lines, respectively (Fig. 5(a)). The mooring system consists of two clusters of six sets of taut mooring lines, meaning twelves mooring lines in total, distributed at 60 ° angles (Fig 4 and Fig. 5(b)). The mooring lines are attached at two heights, one at the bottom of the floater with an angle of attachment of 18.5 ° and one 10 m below SWL with an angle of attachment of 30 ° to give sufficient clearance with regards to the fairlead location and free surface for manoeuvring of vessels near the platform (Fig. 5). The anchor radius is set to be 180 m, to allow the novelty of the anchor sharing concept for multiple turbines installed in an array.

In the taut leg mooring system where the line does not contact the seabed and is taut due to the pretension caused by the platform excess buoyancy, most of the restoring loads are generated by line elasticity. The lines are inclined and the anchor experiences both horizontal and vertical loads. While a single attachment point is modelled, a yaw stiffness is included in the global stiffness matrix that has been approximated based on the methodology presented in [34] for an assumed 20-degree spread of the attachment point, in order to replicate the effects of a bridle/delta connection to reduce the yaw motion of the platform. Fig. 6(a) shows the top view of the mooring configuration circumferentially distributed around the cylindrical floating platform and Fig. 6(b) shows the influence of the angle γ on the mooring system stiffness is investigated at a range of R_C. In this study at R_C=180 m, $\gamma = 20°$ yield almost 8.5 times the yaw stiffness of that at $\gamma = 0°$. as illustrated in Fig. 6(b). The benefit from this configuration is stiffening the yaw mode without affecting the stiffness of other directions.

With increasing numbers of new materials being developed specifically for marine and offshore applications, three materials are considered for the taut mooring system design (steel wire, polyester, and nylon ropes), and their properties are shown in Table 4 [35].

Four mooring lines of 80 mm are assumed to bound together to construct the nylon mooring line, whereas for polyester and steel

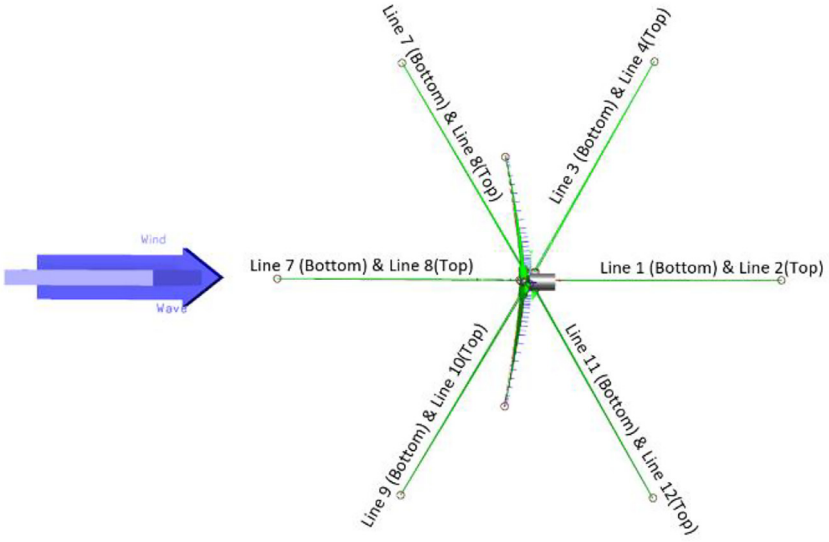

Fig. 4. Mooring Lines Top View.

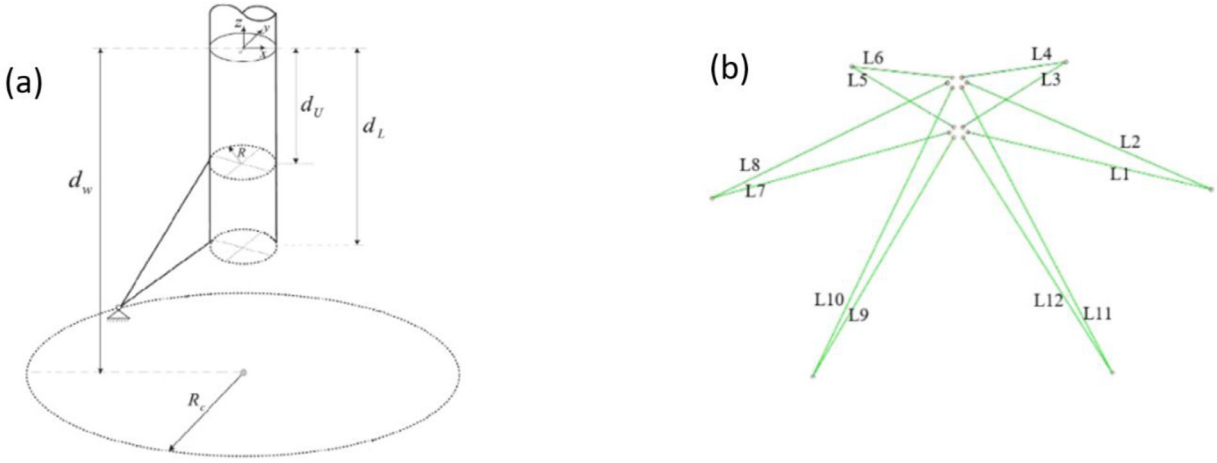

Fig. 5. (a) Taut-Leg Mooring System Configurations (Al-Solihat and Nahon 2016 [29]) & (b) TLB Taut-Leg Mooring Layout.

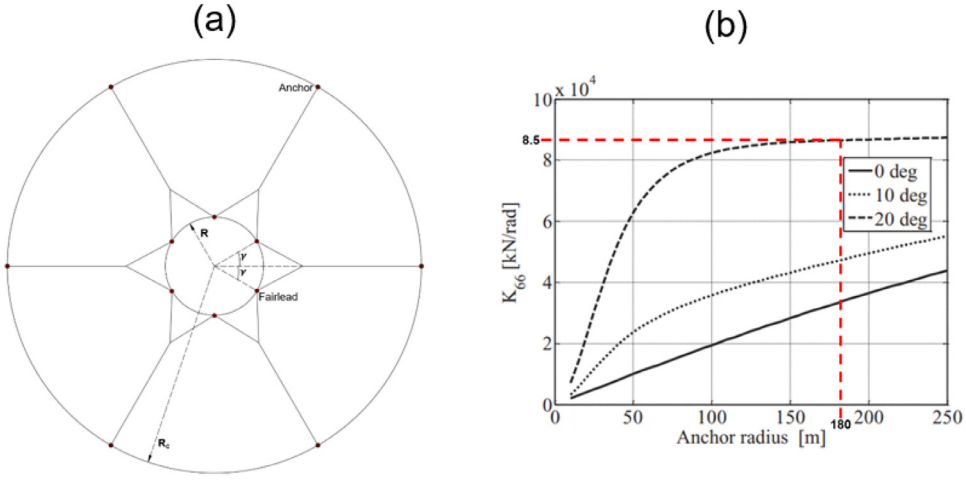

Fig. 6. (a) Top View Taut Mooring System with Bridle Connection Configuration (b) Influence of Mooring System Geometry on the Stiffness (Al-Solihat and Nahon 2016 [29]).

Table 5
Elongation Value Based on MBF [35].

	% MBF	10	20	30	40	50
Polyester	%	0.9	2.6	4.1	5.6	7
Nylon	Elongation	5	7.3	8.6	9.6	10.3

Table 6
Polyester & Nylon Axial Stiffness [46].

Purposes	Static stiffness	Dynamic stiffness (Low and Wave frequency)
Offset	10.MBF	20.MBF
line tension	20.MBF	35.MBF

(Spiral Strand Xtreme 1960 Grade), lines of 310 mm and 240 mm diameter respectively are selected from the catalogue presented by Bridon-Bekaert Ropes Group [35]. The stiffness is calculated based on multiple sections for multiple ropes, which means four mooring lines bonded together as one mooring line. Table 4 shows the detailed characteristics of the mooring lines. The summary of simplified assumptions is considered for mooring system are including uniform mooring line material cross section for calculating hydrostatic stiffness matrix, the quasi- static mooring line model, 20-degree spread of the mooring line attachment point, four mooring lines of 80 mm are assumed to bound together to construct the nylon mooring.

However simplified assumptions considered for mooring line, more detailed description of the mooring line material may reduce the extent of snap loading or including additional damping would have similar effect. These aspects could reduce the accuracy of the predicted hydrodynamic loads exerted on the platform and mooring lines particularly in low and moderate fluid speeds which may affect the resulting system response.

3.3.1. Tension-Elongation of synthetic fibre ropes

The mechanical behaviour of synthetic ropes is more complex than the corresponding behaviour of steel wire ropes. The complexity comes from the synthetic rope's visco-elastic and visco-plastic properties, which allows it to gradually develop permanent increases in length depending on the load history. In practice, this means that a synthetic rope's length and mechanical properties may differ prior to and after a severe loading. Synthetic materials such as polyester and nylon are highly nonlinear and time-dependant load-elongation, which plays an essential role in their performance [36]. Therefore, relevant tests should determine such behaviours before designing and applying those fibre rope mooring components. The offshore industry has studied testing and modelling methods for polyester, and outcomes of several Joint Industry Projects (JIPs) have been integrated into offshore standards such as API-RP-2SM [37], DNVGL-RP-E305 [38], and ABS [39], which methods are perfect examples. However, these methods cannot be applied directly to nylon due to their highly nonlinear load-elongation and complex fatigue behaviours. Besides, using nylon ropes for permanent mooring applications is relatively new to the offshore industry since conventional nylon has a meagre fatigue life. Therefore, it is crucial to focus on the mechanical behaviours of fibre mooring ropes to deal with the modelling concern and verify the safety and cost-effectiveness of the mooring design. DNVGL-RP-E305 [38], Falkenberg et al. [40,41] introduced the concept of the Syrope model (Fig. 7). Falkenberg recommends selecting the working curve for static mooring analysis to determine the floating structure excursions which could account for the maximum historical tension that the rope has been through. DNVGL-RP-E305 requires using a correct dynamic stiffness model to calculate the designed tension responses.

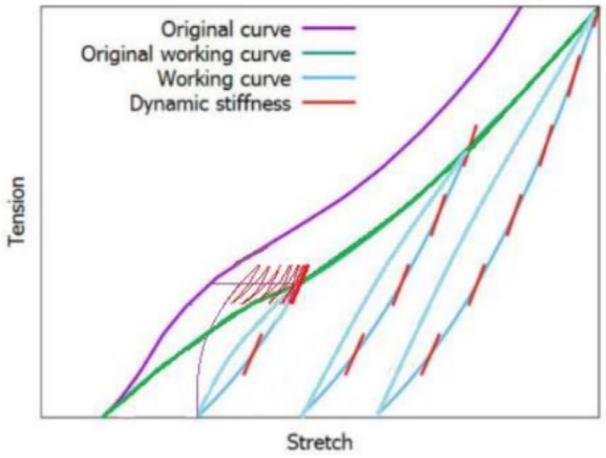

Fig. 7. The Syrope Model (Falkenberg et al. [36,37]).

Table 7
Dynamic Tension-Elongation Inputs in SIMA.

Polyester		Nylon	
Elongation (%)	Tension (N)	Elongation (%)	Tension (N)
0	0	0	0
0.9	2.84E+08	5	2.20E+08
2.6	5.69E+08	7.3	4.41E+08
4.1	8.53E+08	8.6	6.61E+08
5.6	9.96E+08	9.6	7.71E+08
7	1.14E+09	10.3	8.82E+08

Table 8
Platform 6 DOF Natural Period and Damping Ratio.

DOF	Natural Period (rad/s)	Damping Ratio
Surge	0.7853982	0.009533
Sway	0.7853982	0.009833
Heave	1.2566371	0.090136
Roll	0.7853982	0.023202
Pitch	0.8975979	0.024442
Yaw	1.2566371	0.043466

The non-linear material curve used in static analysis is given by shifting the working curve by redefining the initial stress-free length so that the working and original working curves intersect at maximum tension. On the other hand, the linear material curve used in the dynamic analysis is given by dynamic stiffness coefficients using the mean tension of the segment. The initial stress-free length is then redefined such that the tension is identical between static and dynamic analysis, given the elongation of static analysis (see Fig. 7). In SIMA, for fibre rope segments, the average tension over the elements in a segment is used to compute the intersection between the working curve used in static analysis and the linear tension-strain curve used in dynamic analysis.

3.3.2. Dynamic stiffness empirical formula

Generally, the dynamic stiffness of fibre ropes depends strongly on the mean tension, moderately on the tension amplitude and mildly on the loading frequency. The loading frequency and tension amplitude impacts are negligible for polyester [42]. Although Nylon seems to have closely similar behaviours to polyester, its responses are found to be more nonlinear than the latter. The mean tension is the main factor that significantly influences the dynamic stiffness, and the effects of strain amplitude and loading cycles cannot be ignored [43]. The proposed empirical expression of dynamic stiffness for polyester ropes introduced by Fernandes et al. [44]. is expressed in Eq. (15), where $\frac{E}{\rho}$ is specific modulus (N/tex),

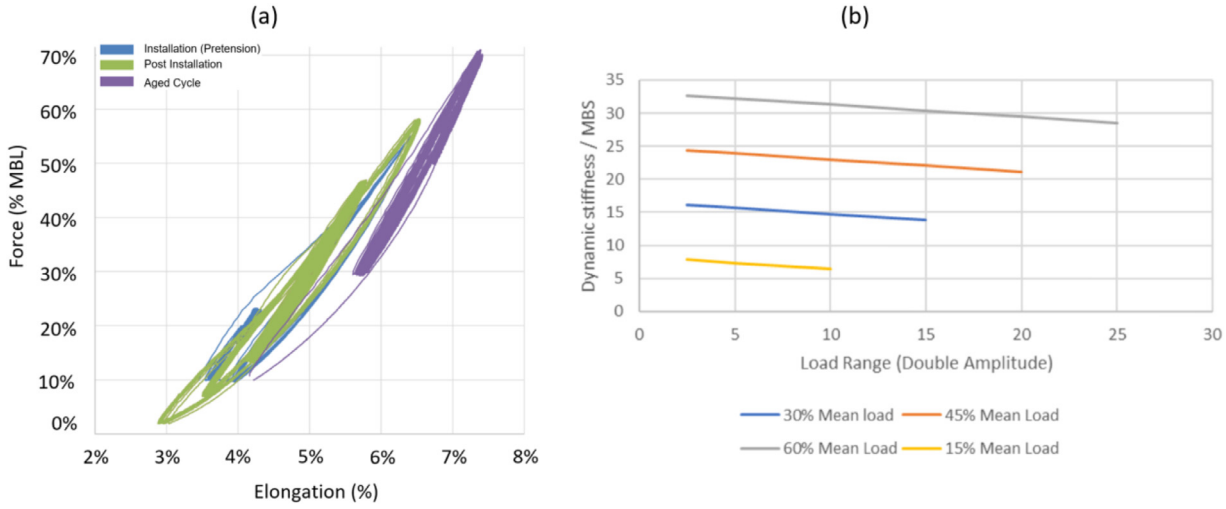

Fig. 8. (a) Polyester and (b) Nylon Dynamic Stiffness Curve (Data obtained from Bridon-Bekaert - The Ropes Group).

L_m is mean load (% of MBL), L_a load amplitude (% of MBL), T_o is the period of loading, and α, β, γ, δ are empirical coefficients. Eq. (16) shows the expression of a non-dimensional axial stiffness of polyester ropes where *MBL* is minimum breaking load, L_a is tension amplitude, l is initial length of the rope, and Δl is the stretch.

$$\frac{E}{\rho} = \alpha + \beta L_m - \gamma L_a - \delta log(T_o) \tag{15}$$

$$K_{rs} = \frac{L_a l}{\Delta l.MBL} \tag{16}$$

Based on dynamic stiffness tests on a wire-lay 3-strand nylon rope carried by Huntley [45], the dynamic stiffness of the nylon rope depends strongly on the applied mean tension and the tension amplitude. Eq. (17) shows expression of dynamic stiffness for nylon rope where a, b, c are determined from a multiple linear regression on the nylon dynamic stiffness testing data reported by Huntley [45].

$$K_{rd} = aL_m - bL_a + c \tag{17}$$

This study used the static and dynamic test outputs of quasi-static and dynamic stiffness for post-installation polyester and nylon ropes provided by Bridon-Bekaert Ropes Group to determine the dynamic stiffness of polyester and nylon ropes. Fig. 8 shows dynamic stiffness curve of (a) polyester and (b) nylon ropes. The dynamic stiffness of nylon rope depending on the tension amplitude, L_a.

The dynamic stiffness of polyester ropes can be two to three times the static stiffness so this must be considered. The static stiffness is utilized for the initial region of the loading curve up to the mean load, followed by the dynamic stiffness which is used to predict the cyclic part of the loading, including low frequency and wave frequencies [39,47]. A mooring line under a severe environment typically experiences a steady mean load and dynamic loads oscillating around the mean load. Typical static stiffness is in the range of 10–20 times MBF, and typical dynamic stiffness is 20–30 times MBF, as shown in Table 6 [39,46]. Ideally, the polyester rope's load–elongation properties should be modelled as nonlinear elastic by expressing the load–elongation relationship [47,48]. This study considered the upper bound and lowered bound approaches to deal with polyester and nylon ropes stiffness, mean that at 10% to 20% of elongation for static stiffness, MBF is multiplied by 10 – 20, whilst at 20% to 50% of elongation for dynamic stiffness, MBF is multiplied by 20 - 35.

Table 5 shows the elongation vs spliced MBF, tested following CI1500B-2015 provided by Bridon-Bekaert The Ropes Group [35]. Unlike steel wire rope, polyester and nylon ropes exhibit axial load–nonlinear elongation characteristics (Fig. 8 and Table 5), depending on loading type and varying with time and loading history.

In SIMA the average tension over the elements in a segment is used to compute the intersection between the working curve used in static analysis and the linear tension-strain curve used in dynamic analysis (See Table 7).

The free decay tests were performed to document the natural period of the system in all 6 DOF using the base floater design and applying initial displacement in all translational and rotational motions through specified forces at the beginning of the time domain simulations.

The natural period and damping ratio of 6DoF are calculated from free decay test illustrate in below Table 8.

4. Methodology and numerical analysis

4.1. Methodology

SIMA is a workbench software that provides a graphical user interface for the use of SIMO and RIFLEX. SIMO and RIFLEX models can be developed and modified without the use of input-files. SIMA also has a built-in tool for the setup of calculations using combinations of different variables, and thus a simple way of running multiple analysis in parallel. Since TD simulations are solved step-by-step, only a single logical processor can be utilized per simulation.

The present numerical simulation is based on the potential flow theory using DNVGL WADAM (Wave Analysis by Diffraction and Morison Theory) [18,49]. The frequency-domain hydrodynamic analysis is initially performed without the mooring lines, and the stiffness for the taut mooring system. Forces and moments are considered in terms of transfer functions. Added mass and radiation damping as hydrodynamic coefficients, wave excitation forces, and response operators are calculated in WADAM, solved by potential theory based on the implementation of 3D panel method and Green's theorem in WAMIT [18,50]. By using WAMIT to solve the first-order problem, outputs include added-mass, damping, and first-order wave excitation force coefficients. The hydrostatic restoring matrix is a default output, and the motion RAOs were chosen as an output. The second order mean-drift force is computed as part of the first-order problem because it only depends on

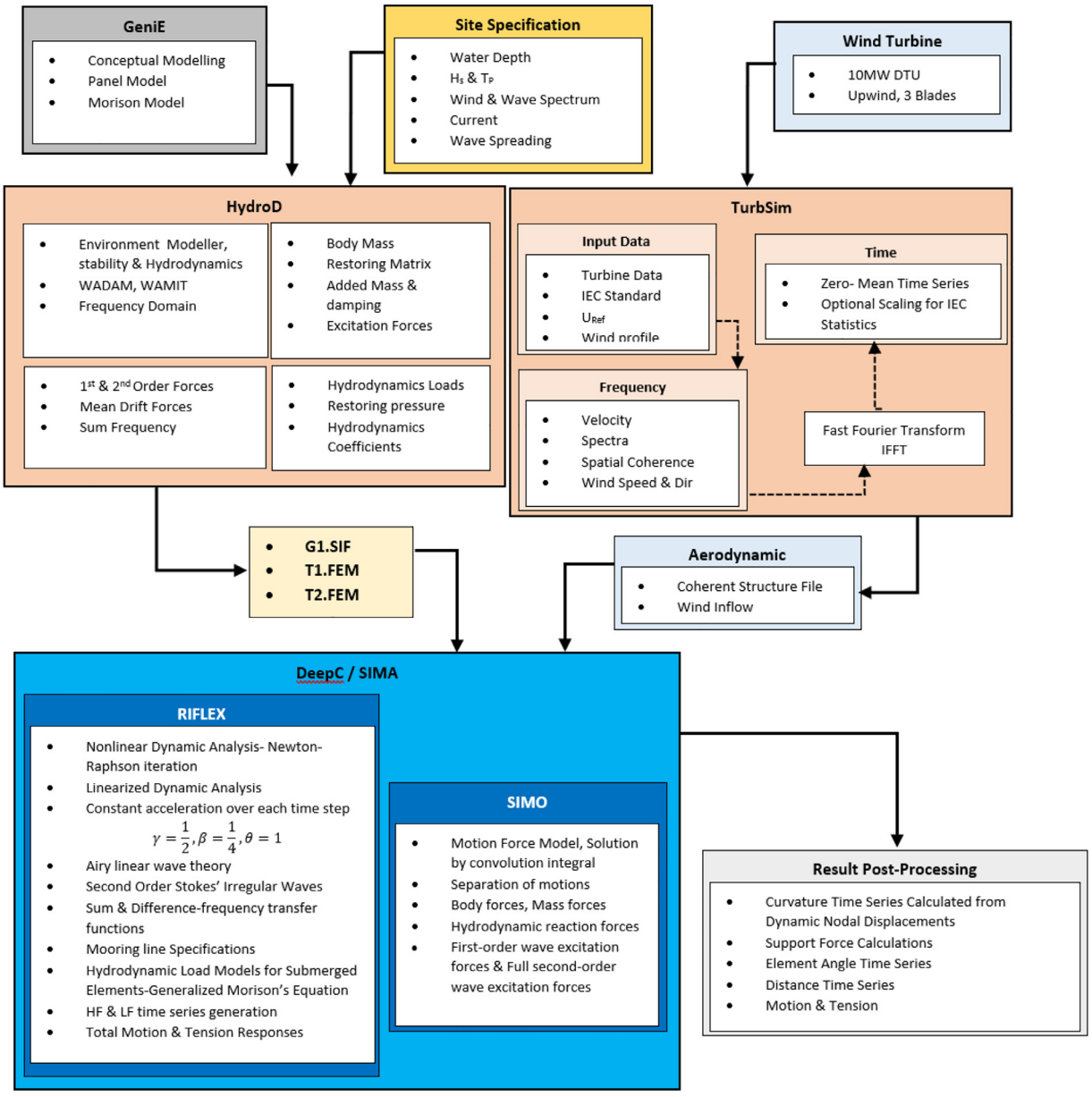

Fig. 9. Methodology Flowchart.

quadratic contributions from the first-order potential. Solving the second-order problem with WAMIT provides second-order force QTFs and second-order motion QTFs. The specific incident wave frequencies and wave headings for which the radiation and diffraction problem are solved and specified come from WAMIT. Fig. 9 shows the methodology and flowchart for the numerical simulation [51–53].

Time-domain analysis was performed in SIMA using SIMO/RIFLEX to obtain the coupled floater and mooring system response results. When computing the coupled motion response and mooring line loads, during time-domain analysis in SIMA, several factors must be considered: specifically, excitation forces, resulting added mass, potential damping matrices, and response amplitude operators up to second order, all in combination with the wave, wind, and current excitation forces, as well as the floating platform's mooring configuration. Results for the dynamic response in terms of both motion and mooring forces are calculated in the time domain in SIMO-RIFLEX [54–56].

The aerodynamic calculations are performed using the blade element method (BEM), considering numerical corrections for stall and wake effects, including dynamic stall and dynamic wake correction. This study is used the external code in TurbSim to generate the Normal Turbulence Wind (NTM) model for operational conditions and the Extreme Wind Model (EWM) with turbulence intensity for survival conditions.

4.1.1. Coupled wind-wave simulation tool

SIMA coupled simulation code was developed by linking the SIMO [19] and RIFLEX [20] hydrodynamic, structural, and control system computational tools, from SESAM package, with the aerodynamic forces and wind field generation capabilities of TurbSim, from NREL [57]. The simulation tool employs the finite element solver available in the combined SIMO/RIFLEX tool, passing position and velocity information to the aerodynamic code at the first iteration of each time step. Then returns, lumped forces along the wind turbine blades. It is assumed that the origin of the body's

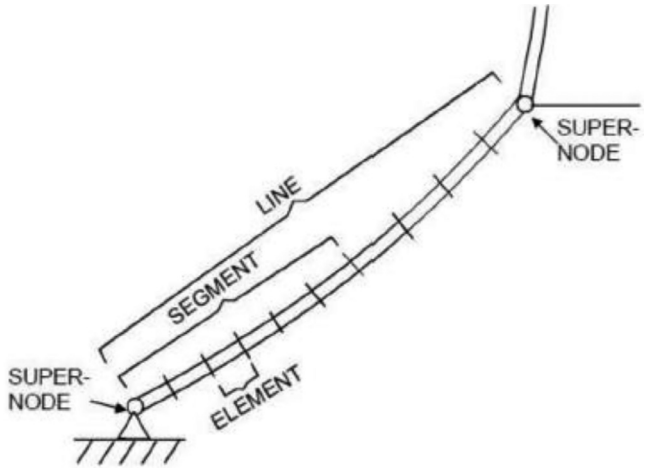

Fig. 10. Definition of Line, Segment, and Element in RIFLEX (Godø 2013).

fixed rotor coordinate system coincides with the hub centre with Z-axis aligned in the direction with the rotor (slow speed) shaft, i.e., from the support to the hub. The wind loads on the blades are computed based on the load coefficient description in the airfoil library file together with a double-multiple stream tube blade element momentum method. The approach includes dynamic stall effects. The nonlinearity sources considered in this study including, nonlinear time domain analysis, nonlinear wave included up to second order, nonlinear free surface and nonlinear fibre mooring lines material curve.

4.1.2. RIFLEX

A RIFLEX model is built with super nodes and lines, where the super nodes functions as the connections in the system. They are position by coordinates and can be given constraints in any of the 6 DOFs as well as prescribed offsets that they are moved to when RIFLEX runs the static analysis. The super nodes are connected to each other by lines, which are defined by line types which again are composites of one or more segments. Each segment can contain a single set of cross-sectional properties, and different cross-sectional properties can be included by dividing a line into several segments. Each segment can be split into multiple elements that are used for the FEM formulation. The relation between line, segment and element is given in Fig. 10 [58].

4.1.3. SIMO

SIMO (Simulation of Marine Operations) is a software developed to simulate motions and behaviour of complex floating vessels and suspended loads, such as an offshore crane loading operation. SIMO uses TD simulation of the motions of SIMO bodies and the forces that act on these bodies. In addition to response calculation, SIMO also have the ability of generating time series of wind, waves and current. For this study, SIMO is used to output the pitch and yaw motion of the COG as well as the generation of environment.

4.2. Numerical analysis

By assuming incompressible, irrotational flow, the fluid velocity vector can be defined as the gradient of the total velocity potential Φ, satisfying the Laplace equation, $\nabla^2\Phi = 0$. The boundary value problem (BVP) will be solved in the following part in both first-order and second-order to investigate the hydrodynamic characteristics of FOWT system. By assuming a small wave slop of incident wave using a perturbation solution, the velocity potential can be expanded in a form state in Eq. (18) [59].

$$\phi(x,y,z,t) = \phi^{(1)}(x,y,z,t) + \phi^{(2)}(x,y,z,t) + \ldots \tag{18}$$

When body is not fixed, the first-order motion affects the second-order solution. By considering the quadratic interaction of the two linear wave components of the frequencies ω_i and ω_j. The second-order velocity potential, $\Phi^{(2)}(x,y,z,t)$, shows in Eq. (19) which it is decomposed into sum $(\omega_i + \omega_j)$ and different $(\omega_i - \omega_j)$ frequency terms where the ϕ_{ij}^{+} and ϕ_{ij}^{-} are referred to the sum and difference frequency [59–61].

$$\Phi^{(2)}(x,y,z,t) = Re\sum_i\sum_j \phi_{ij}^{+}(x,y,z)e^{-i(\omega_i+\omega_j)t} + \phi_{ij}^{-}(x,y,z)e^{-i(\omega_i-\omega_j)t} \tag{19}$$

Taking into account the excitation forces, the resulting added mass and potential damping matrices and response amplitude operators up to second-order in combination with the wave, wind and current excitation forces as well as the floating platforms' mooring configuration allows for computing the motion response and mooring line loads in the time domain analysis in DeepC. The total second-order force can be expresses in terms of incident wave (I) diffracted wave (D), wave radiation (R), hydrostatic restoring force (HS), and $F_q^{(2)}$ represents the second-order force caused by quadratic first-order quantities. whilst $F_I^{(2)} + F_D^{(2)} + F_q^{(2)}$ can be expressed as $F_{Ex}^{(2)}$ which is the second-order wave exciting force, The total second-order force can be also expressed as in Eq. (20) [62].

$$F^{(2)} = F_R^{(2)} + F_{HS}^{(2)} + F_{Ex}^{(2)} \tag{20}$$

As the platform motion can be solve using the hydrodynamic coefficients and wave loads, the equations of motions in frequency domain for the linear wave structure interaction problem can be written as in Eq. (21) [63], Where M is the mass, μ is added mass, C is the hydrostatic restoring, and λ is damping coefficient which are 6×6 matrices. The frequency-domain motion amplitude $\xi(\omega)$ is the 6×1 vector.

$$\left[\left(-\omega^2(M+\mu) + i\omega\lambda + C\right) + \left(-\omega^2\mu + i\omega\lambda\right)\right]\xi(\omega) = F_{Ex}(\omega) \tag{21}$$

To describe the motion equations in time domain the impulse response theory [64] is adopted. The motion equation of platform can be expressed as in Eq. (22).

$$[M+\mu(\infty)]\ddot{x}(t) + \left[\int_{-\infty}^{t} k(t-\tau)d\tau\right]\dot{x}(\tau) + Cx(t) = F_{Ex} + F_W + F_C + F_M \tag{22}$$

The term $\int_{-\infty}^{t} k(t-\tau)d\tau$ describes radiation loads where, $k(t)$ known as the wave radiation retardation kernel and the term $k(t-\tau)$ is the convolution term of velocity that represents the memory effect of the reaction force of fluid dynamics. τ is a dummy variable with the same units as the simulation time, t.

The added mass and damping coefficient are frequency dependant. The radiation loads are obtained in the time domain with hydrodynamic added mass and damping matrices. In this study WADAM is used to calculation of hydrodynamic added mass and damping matrices also excitation forces. According to the impulse theory [64,65], the wave excitation force in frequency domain can be transferred to time domain excitation force. The wave excitation force in frequency domain can be obtained according to the diffraction theory in frequency domain and with multiplying the wave amplitude time history the wave excitation force in time domain can be obtained.

According to the DNV-RP-C205 guideline [66], the wind and current force are calculated by the wind and current coefficients.

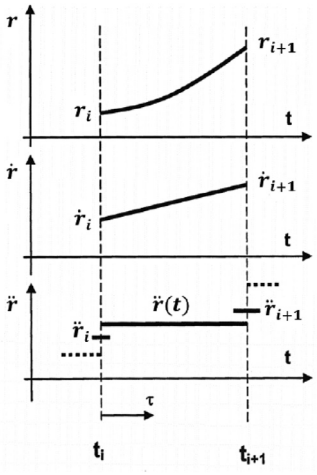

Fig. 11. Constant average acceleration (Larsen 2014).

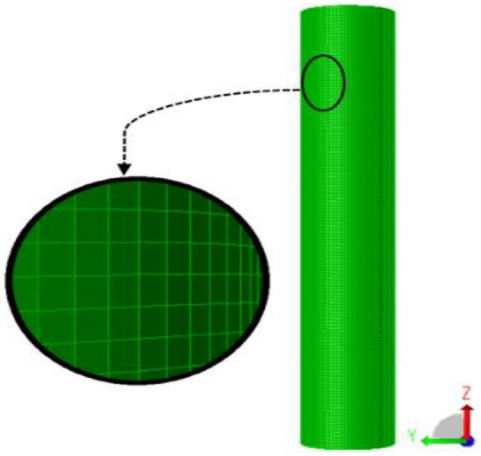

Fig. 12. Mesh Resolution.

The wind and current force express in Eqs. (23) and (24) respectively where C_W is the wind coefficient, ρ_α is the air density, A_W is the shadow area, U is the relative wind speed on the platform, C_C is the current coefficient, ρ_w is the fluid density, A_C is the shadow area in current direction, and V is the current speed.

$$F_{Wind} = \frac{1}{2} C_W \rho_\alpha A_W U^2 \tag{23}$$

$$F_{Current} = \frac{1}{2} C_C \rho_w A_C V^2 \tag{24}$$

The mooring system is very important to keep the floating platform stable under wind, waves, and current effects. Mooring components are the number of cables that are connected to floating platform and the anchor is connected to seabed. Mooring system cables are made from different materials, and these could be chain, steel, or composites. The tension on the cables is important to keep the platform stable under environment conditions and it is dependant on cable elasticity, location in water, cable weight in the water, extensional stiffness of cable and number of cables. The total load on the platform from all mooring lines is defined in Eq. (25) where F_M is the component of total mooring system, $F_{Pre-tension}$ is the pre-tension of lines from the weight of the cable not resting on the seafloor if the lines are buoyant $F_{Pre-tension}$ should be zero, and $C_{Elastic\ Stiffness}$ is the elastic stiffness of the mooring lines and the effective geometric stiffness by the weight of the cables in water also depends on the layout of the mooring system [20].

$$F_M = F_{Pre-tension} - C_{Elastic\ Stiffness} \tag{25}$$

4.2.1. Non-linear time domain simulation

In the present work, the focus is on the hydrodynamic forces on the platform and its response which cannot be computed accurately without accounting for static and dynamic effects of the tower, nacelle and rotor, wind forces, and the forces from the mooring lines. A fully resolved computational model of the full platform may be possible but would certainly be very demanding on computational resources. It is likely, however, that the elasticity of the tower, for example, plays only a small role in determining the response of the platform to wave loading. Similarly, using simplified models for other aspects, such as the wind load and the tethers, is unlikely to change the results we are interested into any significant degree.

The most important advantage of running a TD simulation is considering the non-linearities. The step-by-step numerical integration of the incremental dynamic equilibrium equations allows for incorporating these non-linearities. The numerical integration is solved with a Newton-Raphson equilibrium at each time step. The downside of a TD simulation is that it is time-consuming due to the repeating generation of the stiffness, mass, and damping matrices. The hydrodynamic loading on the elements is computed using panel model to calculate the hydrodynamic responses from potential flow and the drag term in Morison's equation as shown in Eq. (26). F_H is the total hydrodynamic forces, $F_{Potential}$ is the sum of potential flow forces, $F_D$is the drag force, F_{FK} is the potential flow force contribution from Freude-Kriloff, F_S is the potential flow force contribution from diffraction, F_R is the Potential flow force contribution from added mass and damping.

$$F_H = F_{Potential} + F_D = F_{FK} + F_S + F_R + F_D \tag{26}$$

The method of analysis used in nonlinear dynamic analysis follows the approach outlined by Langen and Sigbjørnsson (1978) [67]. It is assumed that the tangential mass, damping and stiffness matrices are recalculated at each iteration cycle, which will give a Newton-Raphson iteration procedure. A modified Newton-Raphson procedure can also be included by keeping the matrices constant over several iteration cycles. Contributions to the external load vector from prescribed displacements due to vessel motions are applied at each time step. There are, however, no contributions from prescribed displacements in the external load vector during the equilibrium iteration.

4.2.2. Dynamic time domain integration

Eq. (27) shows the expression of the governing dynamic equilibrium equation.

$$R^I(r, \ddot{r}, t) + R^D(r, \dot{r}, t) + R^S(r, t) = R^E(r, \dot{r}, t) \tag{27}$$

R^I represents inertia force vector, R^D is the damping force vector, R^S is internal structural reaction force vector, R^E is the external force vector, t is the time, and $r, \dot{r}, \ddot{r}$ are structural displacement, velocity, and acceleration vectors respectively. The external force vector accounts for weight and buoyancy; drag and mass force from Morison equation; and the aerodynamic force.

The dynamic equilibrium equation is solved in TD using Newmark-β step-by-step integration. Using a constant time step throughout the simulation. This method uses relation between displacement, velocity, and acceleration at time t and $t + \Delta t$ express in Eq. (28).

$$\begin{aligned} \dot{r}_{\,t+\Delta t} &= \dot{r}_{\,t} + (1-\gamma)\ddot{r}_t \Delta t + \gamma \ddot{r}_{t+\Delta t} \Delta t \\ r_{\,t+\Delta t} &= r_t + \dot{r}_{\,t} \Delta t + \left(\frac{1}{2} - \beta\right)\ddot{r}_t \Delta t^2 + \beta \ddot{r}_{t+\Delta t} \Delta t^2 \end{aligned} \tag{28}$$

where γ and β are parameters that define the functional change in displacement, velocity, and acceleration in the integration method. The numerical damping of the method is determined by γ. The integration method is unconditionally stable for $\gamma > \frac{1}{2}$ and $\beta \geq \frac{1}{4}(\gamma + \frac{1}{2})^2$. This study has utilized the constant average acceleration method with $\gamma = 0.256$ and $\beta = 0.505$, introducing a small amount numerical damping to the simulation. This numerical damping does not provide any significant damping to the system when performing the analyses but avoids numerical instability in the calculations. The time step utilized is 0.005 s, as recommended in SIMA for FOWTs. The constant acceleration method is based on taking the acceleration to be constant in the time step [68] as shown in Fig. 11.

The sequence of calculations for the nonlinear integration procedure including equilibrium iteration is summarized in the following:

- Establish integration constants based on the integration parameters.
- Establish initial conditions.
- Calculate the effective stiffness matrix.
- Calculate the effective load vector.
- Compute the incremental displacement.
- Calculate velocity and acceleration.
- Perform the equilibrium iteration.
- Establish the effective stiffness matrix based on the tangential mass, damping and stiffness matrices at iteration i.
- Calculate the effective residual load vector.
- Compute the additional displacement increments.
- Calculate the improved displacement increment.
- Calculate velocity, acceleration, and displacement vector.
- Test for convergence.

5. Verification and validation

5.1. Verification

Due to lack of field measurement at this stage, laboratory model tests are planned to verify the numerical modelling for this specific case. A mesh sensitivity study is carried out to verify the numerical model including the second-order free surface.

Table 9
Mesh Options.

NO Element/Quarter	Mesh Size (m)
113	3
1009	1
2182	0.7
3200	0.6
4482	0.5
5537	0.45

Table 10
Free Surface Mesh Cell Numbers.

Mesh Case	Cell NO
MC1	2000
MC2	2275
MC3	2438
MC4	2460
MC5	2465

5.1.1. Panel model convergence

A mesh sensitivity study for the simulation with different levels of mesh resolution has been carried out. Table 9 represents six options for column surface. Fig. 12 shows an example of submerged columns with a 0.6 m mesh resolution.

The influence of different mesh sizes on the motion response results for heave, pitch, surge, and yaw motions is shown in Fig. 13. This indicates that the system motion responses have reached the stabilised peak amplitude for a mesh size of 0.7 m and below.

The results of mesh convergence on forces, added mass and potential damping show that the model is converged by 0.7 m mesh size. Therefore, based on the mesh convergence study, the final panel model of the TLB floating structure will consist of 3200 elements per quarter (12,800 in total) minimum panels required, each of 0.7 m mesh size, therefore keeping computational costs minimised as far as possible.

5.1.2. Mesh convergence for free surface

The free surface discretisation is required to calculate the second-order velocity potential. Mesh convergence is tested for five different mesh cell numbers, as presented in Table 10, whilst Fig. 14 shows a free surface mesh consisting of 2438 elements per quarter (9750 total mesh cells).

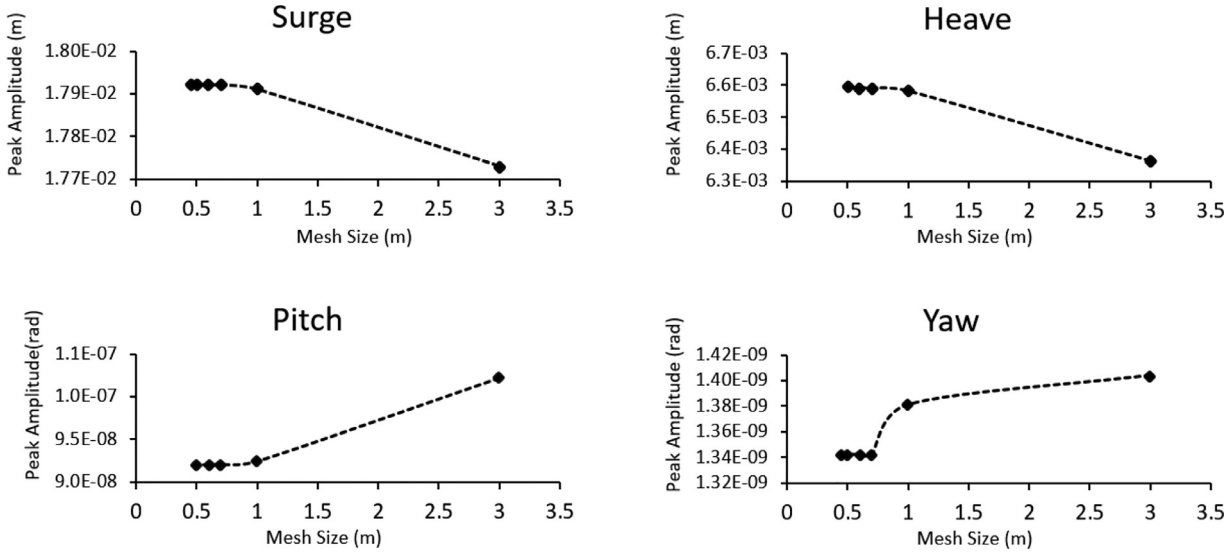

Fig. 13. Motion Response Mesh Convergence.

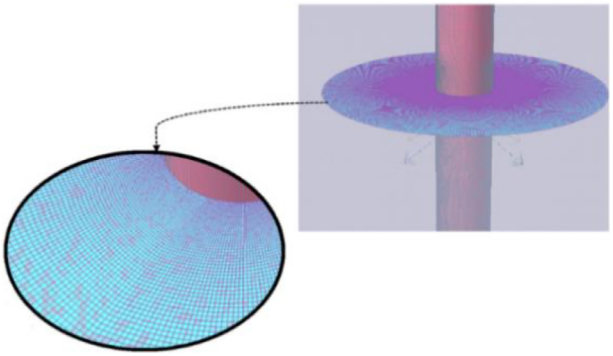

Fig. 14. Free Surface Mesh Resolution.

The effect of various free surface mesh sizes on the pitch, surge and yaw motion responses is presented in Fig. 15. This shows total cell numbers beyond 9750 mesh cells has negligible impact on the amplitude of the forces. The peak values of the second-order force amplitude for surge, pitch, and yaw shown in Fig. 15 approach their convergence point with 2438, 2460, and 2465 elements per quarter, respectively. Hence, a free surface mesh consist of 2438 elements per quarter (9750 total mesh cells) is selected.

5.2. Validation

The validation for the TLB platform was challenging due to a lack of supporting documents and data. This study validates the software set up for the TLB platform based on an experimental study carried out by Berg [16], where three prototype support platforms were investigated experimentally. The TLB 10MW platform is a simple cylinder like TLB S design. The model TLB S platform is attached to the tank base using two sets of steel wire ropes. The mooring system consists of two clusters of three sets of taut mooring lines, which implies six mooring lines in total, distributed in two clusters of lines at 120 ° angles.

A regular wave with a significant wave height of 0.5 m and a period of 2.5 s represented the wave load. The comparison between the simulated results of the Berg study and the simulated results obtained from this study is presented in the following figures. Fig. 16 shows the results of the surge, sway, and heave motion responses simulated in SESAM by this study (black colour dotted lines). UX, UY, and UZ are the translational responses and ROTX, ROTY, and ROTZ are the translational responses results from simulation carried out in the Berg study. By comparing the translational response results present in Fig. 16, however the shapes of the surge and heave responses are similar to the Berg results, it can be noted that the magnitude of the surge and heave are greater than the results from Berg Study simulation. It also can be seen the phase offset between the Berge simulation and the SESAM simulation. The agreement between results is very good, with only small differences in the peak responses but very close alignment of the motion in all three translational motions.

Comparing the rotational responses in Fig. 17, the results of the simulations in this study display the same trend as the results of simulations from the Berg study. Similar to the translational results, however there are slight phase differences, the agreement between rotational results is very good. The magnitude of the pitch and yaw motion responses provided by SESAM simulation are greater than the Berg simulation.

Lower and upper mooring lines tension results are presented in Fig. 18 and Fig. 19 respectively. Berg Study is used the index 1 to 3 is refer to force on mooring lines. Force1 means force on mooring line 1 and so on. Lines 1 to 3 are the lower lines, and Lines 4 to 6 are the upper mooring lines. The dotted lines representing the SESAM simulation results which carried out by this study and solid line is the results from Berg study. It can be seen that the results of both studies have the same shapes and agree very well throughout the simulation times. The mooring tension magnitude provided by SESAM simulation are greater due to having greater motion responses.

However, a small phase offset was observed, with the phase offset occurring in the upper lines more than the lower lines which could be due to line modelling and data recording differences between experiment and simulation. The mooring lines cross-section is assumed to be a beam element, like in the Berg study, but the number of elements defined for the lines can differ. In this study, the number of elements defined for upper lines is 28 and for lower lines is 14.

By comparing the results of TLB S design from SESAM simulation with Berg simulation, the agreement between motion response and mooring line loads results are showing very good agreements.

6. Results and discussion

This section will present and discuss the numerical results of the coupled system of a 10 MW DTU turbine supported by a TLB platform moored with the newly designed taut mooring system

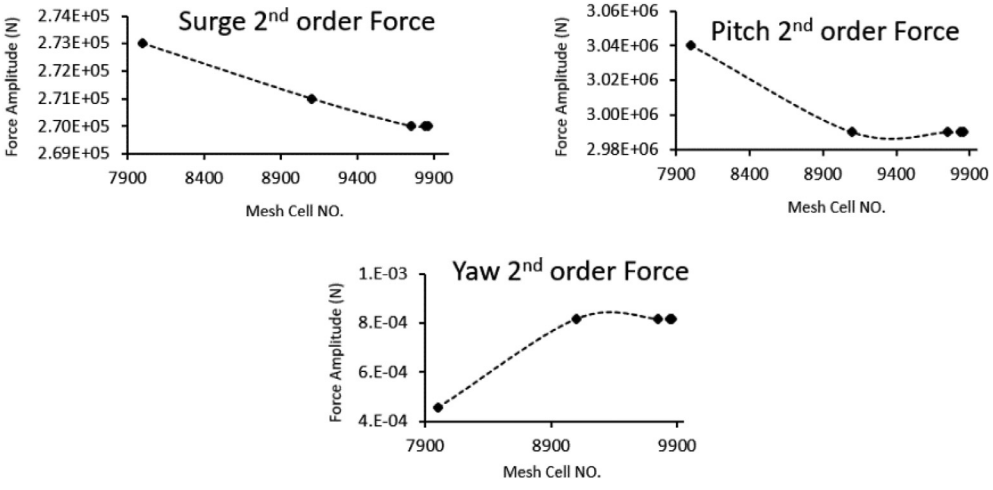

Fig. 15. Second Order Free Surface Mesh Convergence.

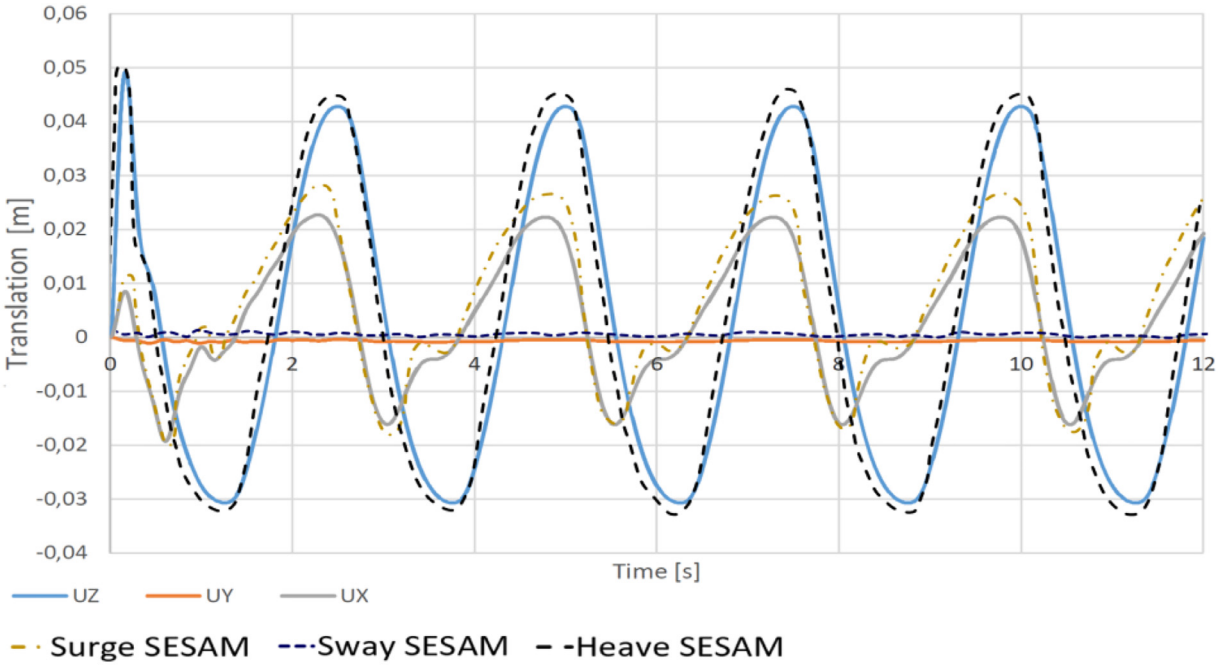

Fig. 16. Comparison of Translational Responses.

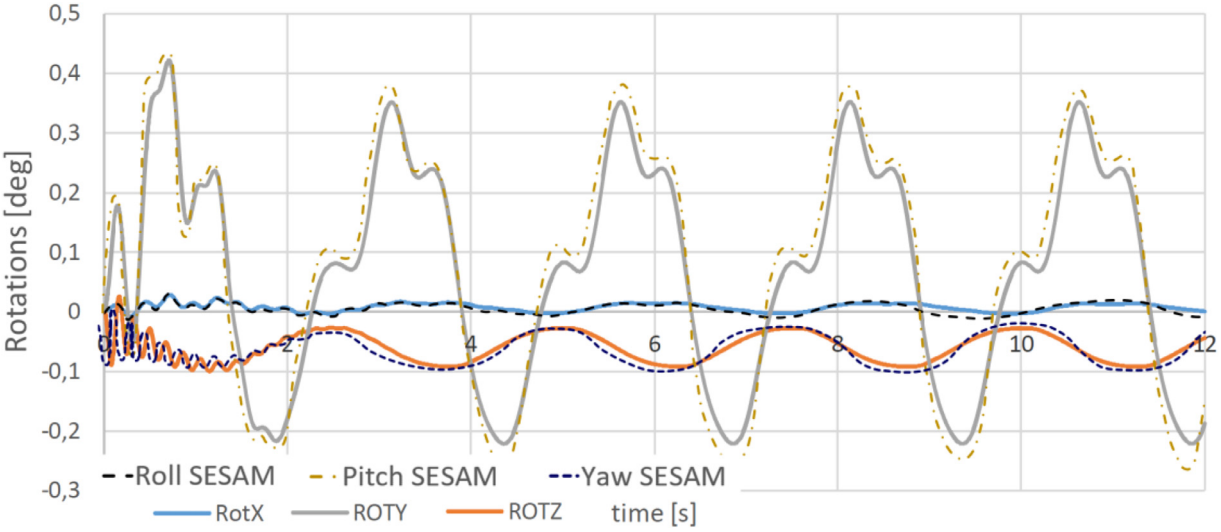

Fig. 17. Comparison of Rotational Responses.

of three different types of materials to the seabed in a systematic manner.

Numerical results are analysed and presented for all load combinations in terms of the motion response of the TLB and the dynamic tension characteristics of the most loaded line. For further design optimisations, the maximum design tension for mooring lines is based on the results obtained during extensive time domain numerical simulations for various environmental conditions according to DNVGL-OS-J103 & J101 [22,69]. Table 11 shows a summary of the DLCs.

The results will be evaluated according to the DNVGL-RP-0286 [70] rules and regulations, specifically the serviceability limit state recommended values for motion responses and nacelle acceleration. The rule-based limitations on response motion as set by DNVGL-RP-0286 [70], imply that the inclination of tilt is limited to 5° (mean value) and 10° (max. value) during operational condition and 15° (max value) for the period of non-operational condition. According to DNVGL-ST-0437 [28], the angle of inclination after damage (idling with fault event) shall not be greater than 17° The assessment of the motion responses will be based on these criteria. Furthermore, following DNV-OS-J103 [69], the design tension, T_d, can be calculated by Eq. (29) where γ_{mean} and γ_{dyn} are load factors given in Table 12, $T_{c,mean}$ is the characteristic mean tension, and $T_{c,dyn}$ is the characteristic dynamic tension.

$$T_d = \gamma_{mean}.T_{c,mean} + \gamma_{dyn}.T_{c,dyn} \tag{29}$$

For ultimate limit state (ULS), $T_{c,\ mean}$ should be taken as the maximum loaded line tension and environmental loads with a 50-year return period. $T_{c,dyn}$ should be taken as the worst dynamic part of the line tension caused by oscillatory LF and WF excitation with a 50-year return period. For accidental limit state (ALS), the components are to be found through a similar deduction, but with a 1-year return period.

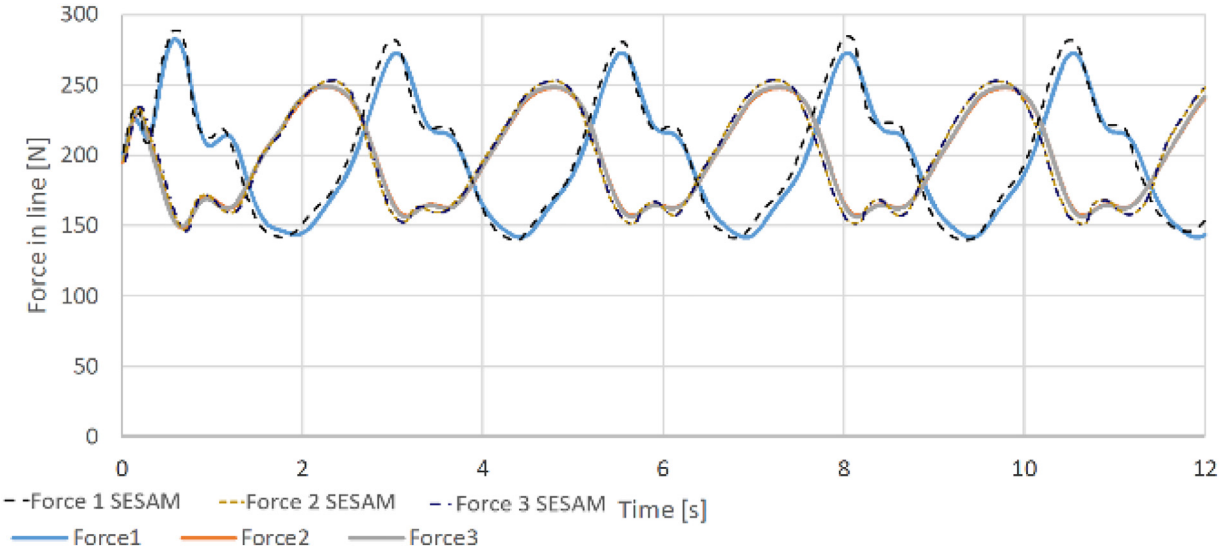

Fig. 18. Lower Mooring Lines Tension Comparison.

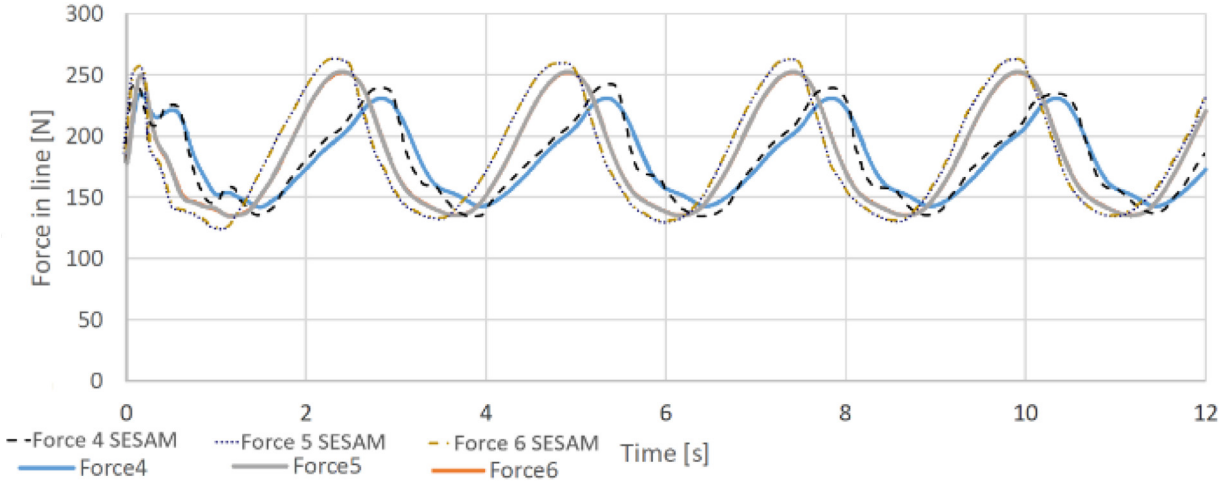

Fig. 19. Upper Mooring Lines Tension Comparison.

Table 11
Summary of Design Load Combinations.

DLC	Wind		Wave			Current
	Model	Speed (m/s)	Model	H_s (m)	T_P (s)	Max Speed at SWL (m/s)
1.1	NTM	11.4	NSS	4.2	9.4	$U_{Wind,50yr} = 0.442$
1.6a	NTM	18	SSS	8.8	13.5	
6.1a	EWM, Turbulence	51.6	ESS	16.8	18.7	$U_{Tidel,50yr} =$
6.2a	EWM, Steady	51.6	ESS	16.8	18.7	1.42
7.1a	EWM, Turbulence	51.6	ESS	11	15.1	$U_{Tidel,1yr} = 0.78$
7.1b	EWM, Steady	50.4	RWH	8.8	13.5	

The characteristic capacity of the mooring lines, S_C, is given in DNV-OS-J103 [69] shows by Eq. (30) where S_{mbs} is the minimum breaking strength (MBS).

$$S_C = 0.95 S_{mbs} \tag{30}$$

The design criterion for ULS and ALS is given in DNV-OS-J103 as express in Eq. (31).

$$S_C > T_d \tag{31}$$

6.1. Static positioning

The characteristics of the mooring lines vary according to the material used. The hydrodynamic coefficients for each system must be calculated for the correct draft of the floater. To achieve the same draft regardless of the mooring line material, the pretension for the lines must be calculated. The static stiffness matrix is calculated for each mooring material as calculated and referenced previously (see Section 3.3). The static positioning of the system moored with three different line materials are listed in Table 13 showing that all three configurations have the same draft.

Table 12
Mooring Lines Design Load Factor Requirements.

Limit State	Load Factor	Safety Class	
		Normal	High
ULS	γ_{mean}	1.30	1.50
ULS	γ_{dyn}	1.75	2.2
ALS	γ_{mean}	1.00	1.00
ALS	γ_{dyn}	1.10	1.25

Table 13
Static positioning of TLB Attached to Seabed with Three Different Mooring Lines.

	X (m)	Y (m)	Z (m)
Steel	0	0	−0.0018
Polyester	0	0	−0.0016
Nylon	0	0	−0.0015

6.2. Dynamic analysis

The primary objective of this section is to assess the TLB dynamic performance under different environmental conditions investigating how different mooring materials could have impact on the dynamic performance.

6.2.1. Operational condition

Two design load case representing Normal Sea State (NSS) and Severe Sea State (SSS) to investigate the TLB system operational conditions. The primary aim is to investigate whether the TLB system with three mooring materials will produce power in severe environmental state. The results for steel, polyester, and nylon mooring lines will be compared and discussed. The maximum load occurred on line 8 (see Fig 4 & Fig. 5(b)) for the three mooring materials in the normal operation events. By comparing the statistical results presented in Table 14, it can be seen that the tensions of the three-line materials are closely related to the surge motion, since a colinear environment with 0° direction caused a maximum surge and the timing of maximum tension corresponds to the timing of the maximum surge displacement.

Figs. 20–24 show that the motion responses of the TLB design when using steel, Polyester, and nylon mooring under DLC1.1. As anticipated with more elastic mooring material, the platform with nylon rope achieved significant increasing in peak motion responses due to nylon's elongation characteristics.

From Fig. 20(a) can observe that the overall shape and distribution of surge responses are similar for polyester and nylon ropes. The surge response median of polyester and nylon are identical, but there are more outliers in the nylon case. The TLB with nylon experienced more fluctuated in surge direction and experienced larger maximum and minimum surge amplitude than the polyester. In terms of heave response Fig. 20(b), the violin plots corresponding three different distributions regards to steel, polyester, and nylon show that the means and interquartile ranges are not very different between three distributions, but the shape of the distributions are different. This means that TLB with steel has less oscillating in heave direction and maximum and minimum heave response are close to mean due to the material rigidity characteristics. Whilst the platform has more freedom with more elastic materials.

The Fig. 20(c) shows that the data is clustered up means that the pitch response of three mooring materials has skewed up gradient during the simulation length. The pitch response of TLB with nylon having a high gradient before stabilising, while the pitch response of the TLB with polyester and steel ropes rises more gradually, before it stabilises. The slope of the TLB with steel rope changes minimally, before becoming constant (see Fig. 23). The TLB with nylon is more oscillating in pitch direction that the TLB with polyester rope. The oscillation of the TLB with steel wire rope in pitch direction is the lowest amongst other mooring materials.

The results of yaw response observed from Fig. 20(d) and Fig. 24 show that the yaw motion amplitude is increased when changing the material from steel to polyester and nylon. The pattern of yaw motion of the TLB with nylon and polyester is almost identical; however, the magnitude of the yaw motion response of the TLB with steel rope is much less than the TLB with fibre ropes. A possible explanation is the assumption made to have a 20° spread of the fairlead attachment to replicate the effects of a bridle/delta connection to reduce the yaw motion of the platform where the mooring line material is assumed to be a steel rope, may not be the most suitable arrangement for the polyester and nylon lines. Hence, the methodology applied to the stiffness to model a bridle/delta connection may have to be revised according to the material to achieve similar motion response.

Fig. 25 shows the most loaded line time history. Although the pattern of response for three mooring materials almost identical, the magnitude of the steel is significantly larger than the nylon rope due to rigidity of the material and the axial stiffness calculated. The axial stiffness of the steel mooring line is constant through the simulation length whilst the axial stiffness of the fibre mooring lines will varied depend on the line elongations.

Table 14
TLB Motion Responses and Maximum Loaded Line (Line 8) Tension Characteristics of Steel, Polyester, and Nylon Mooring Lines for DLC1.1.

	DLC 1.1 (NTM), V_{wind}=11.4 (m/s) H_s=4.2 (m) T_p=8.3 (s)					
		Time (s)	Max	Min	Mean	Std. Dev.
Steel	**Surge(m)**	10,227	1.21	−0.42	0.52	0.22
	Heave(m)	9678	0.38	−0.52	−0.06	0.12
	Pitch(deg.)	10,794	0.46	−0.01	0.36	0.12
	Yaw(deg.)	10,438	0.59	−0.50	−0.12	0.32
	Tension(tons)	10,227	871	510	727	43
Polyester	**Surge(m)**	10,227	2.09	−0.77	0.84	0.39
	Heave(m)	9677	0.62	−0.83	−0.04	0.20
	Pitch(deg.)	10,794	0.62	−0.01	0.45	0.17
	Yaw(deg.)	10,440	0.68	−0.65	−0.16	0.41
	Tension(tons)	10,227	752	435	613	41
Nylon	**Surge(m)**	10,227	2.51	−1.06	0.92	0.49
	Heave(m)	10,238	0.92	−1.16	0.01	0.25
	Pitch(deg.)	10,794	0.95	−0.01	0.62	0.26
	Yaw(deg.)	10,273	1.00	−0.94	−0.21	0.47
	Tension(tons)	10,227	669	353	525	42

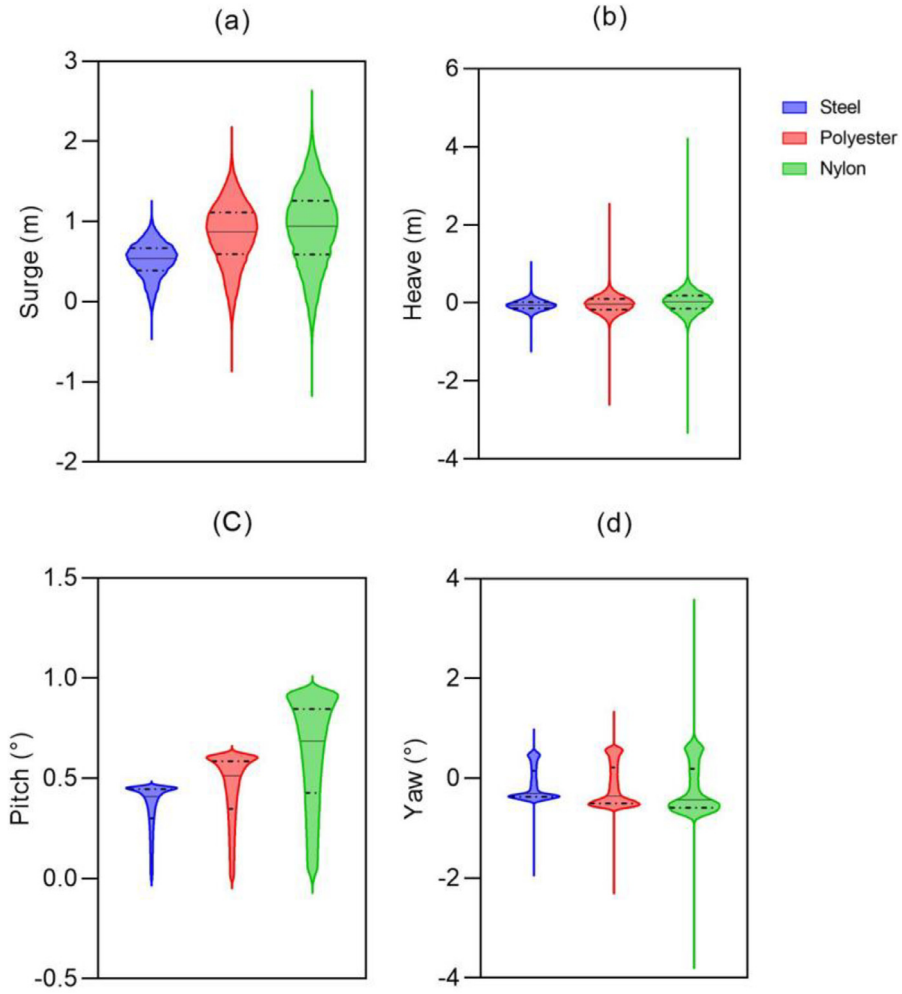

Fig. 20. Violin Plots of the Platform (a) Surge, (b) Heave, (c) Pitch, and (d) Yaw When Using Steel, Polyester, and Nylon Mooring Materials Under DLC1.1.

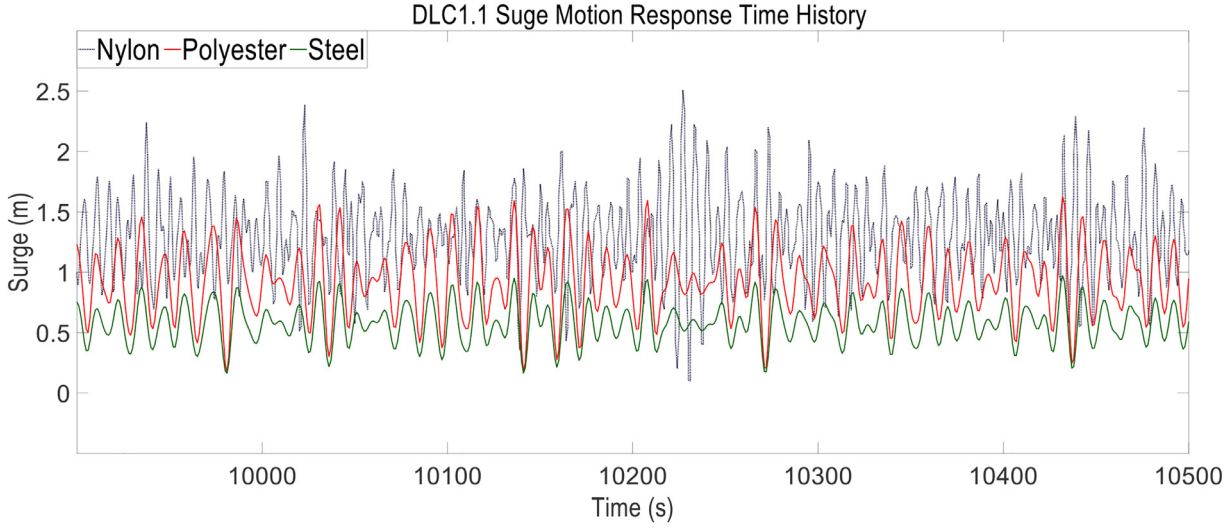

Fig. 21. DLC1.1 Time History of Surge Response for TLB with Nylon, Polyester, and Steel Wire Mooring Lines.

Fig. 26 shown that the surge responses pattern of the TLB with fibre mooring lines are similar whilst the TLB with nylon rope has higher magnitude due to nylon tabular stiffness elongations inputs. Although the TLB moored with the steel mooring line has experienced smaller surge amplitude than polyester and nylon ropes, it exhibited the highest tension, as would be expected due to the increased axial stiffness of the material. The polyester material is more rigid than the nylon material, thus, the TLB is seen undergoing the highest surge motion while using nylon rope due to the elasticity of the nylon material. Comparing the elon-

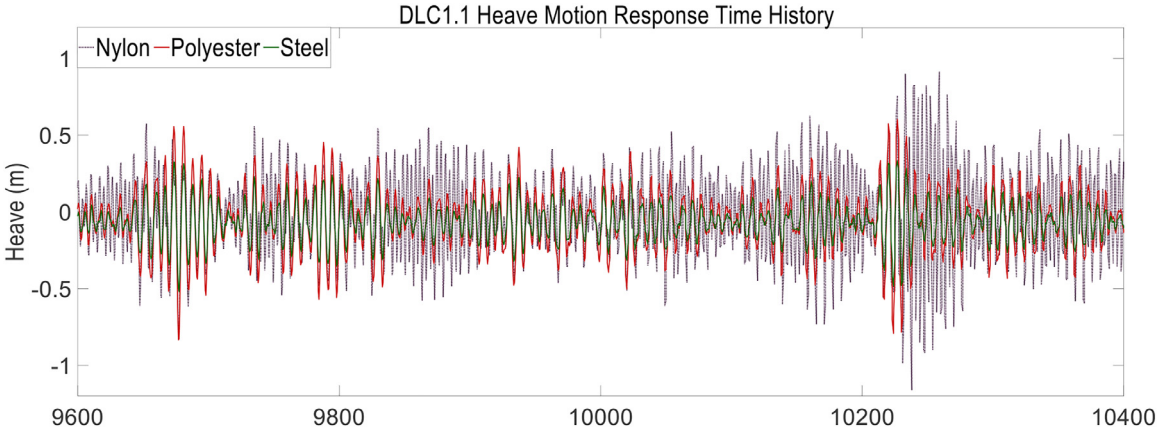

Fig. 22. DLC1.1 Time History of Heave Response for TLB with Nylon, Polyester, and Steel Wire Ropes.

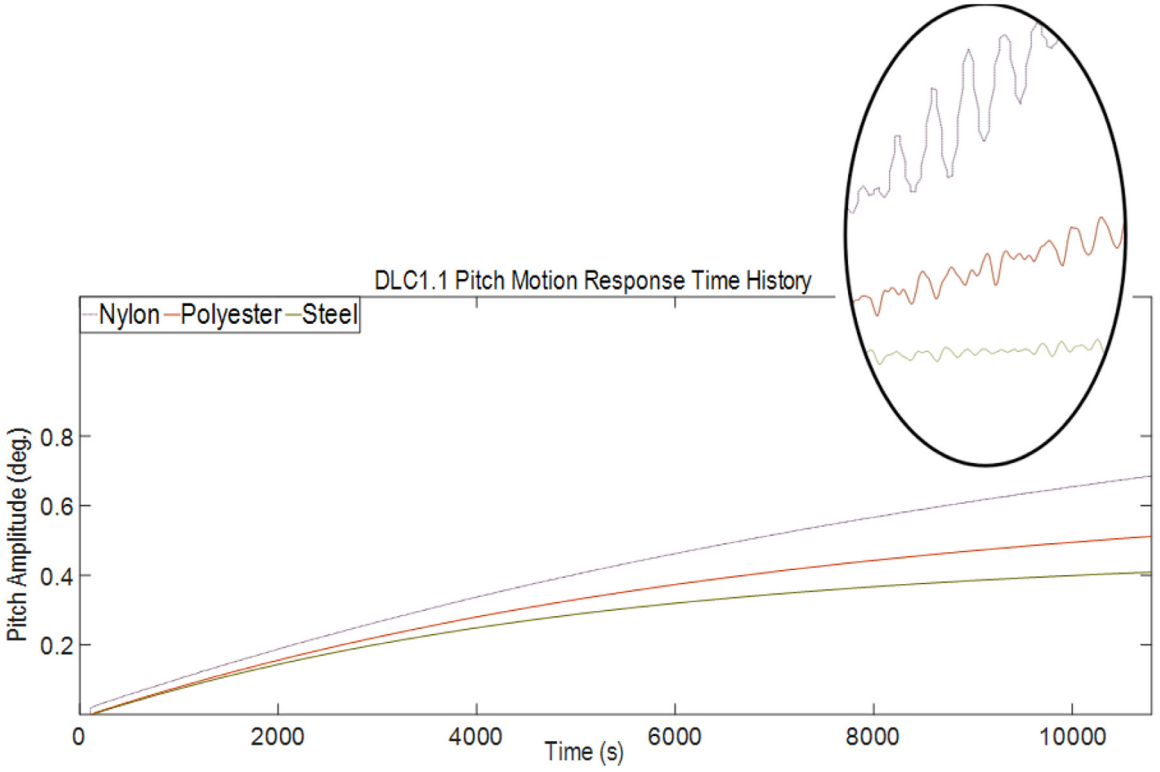

Fig. 23. DLC1.1 Time History of Pitch Response for TLB with Nylon, Polyester, and Steel Wire Ropes.

gation characteristics of the nylon and polyester ropes presented in Table 5 showed that the nylon rope is elongated 73% and 42% more in the calculated static and dynamic stiffness respectively, compared to the polyester rope at the same percentage of MBF.

The performance of the TLB under DLC1.6a event was considered to determine the operational performance boundaries of the system with three mooring materials. The primary objective of 3-hour environmental conditions defined for DLC1.6a was to investigate whether the TLB with three mooring materials would operate in power generating phase safely up to which significant wave height represents severe sea state and, second, satisfy rule base limitation. Similar to the results obtained for DLC1.1, surge motion response and dynamic tension occurred concurrently for the three-line materials, indicating that the surge motion of TLB and dynamic tension of the most loaded mooring line are strongly coupled, and dependant on environmental condition. The fluctuations around the mean offset position of the TLB are reduced with steel mooring lines compared to nylon and polyester (see Table 15).

According to Fig. 27, the fluctuations around the mean offset position of the TLB are reduced with steel mooring lines compared to nylon and polyester. Further indicating that the elasticity of the mooring line significantly affects the dynamic behaviour of the platform. The fluctuations in load however are more significant for the steel mooring line with an increased standard deviation compared to the other two mooring systems. It is noted that the TLB with steel mooring line has less surge oscillation than that with fibre mooring lines, likely due to the mooring line material's elasticity whilst the dynamic tension in the maximum load steel mooring line is the highest, and the lowest is the nylon mooring line.

The increased pitch motion of the TLB with Nylon mooring lines compared to the other two configurations, across both operational

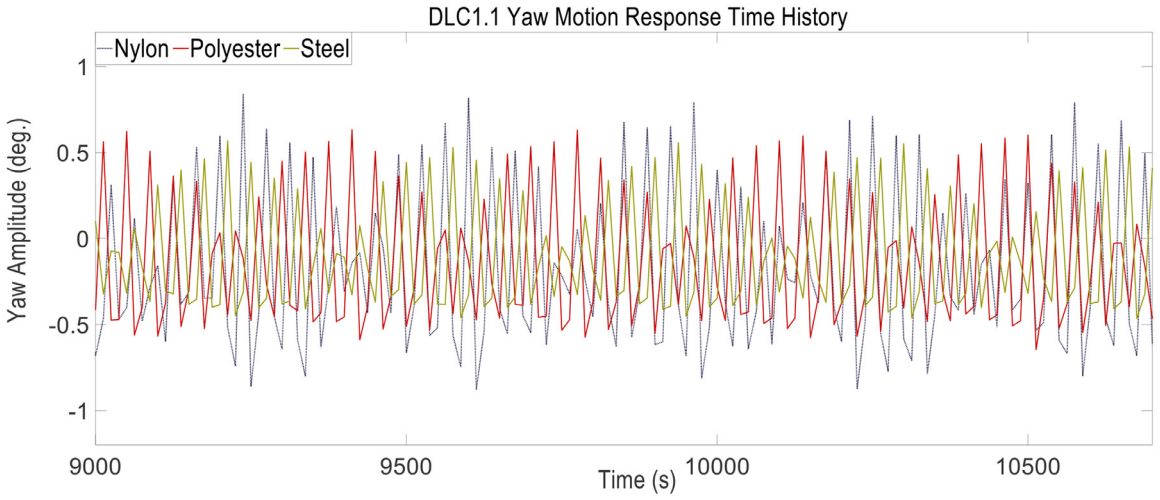

Fig. 24. DLC1.1 Time History of Yaw Response for TLB with Nylon, Polyester, and Steel Wire Ropes.

Fig. 25. DLC1.1 Time History of Tension Response for TLB with Nylon, Polyester, and Steel Wire Ropes.

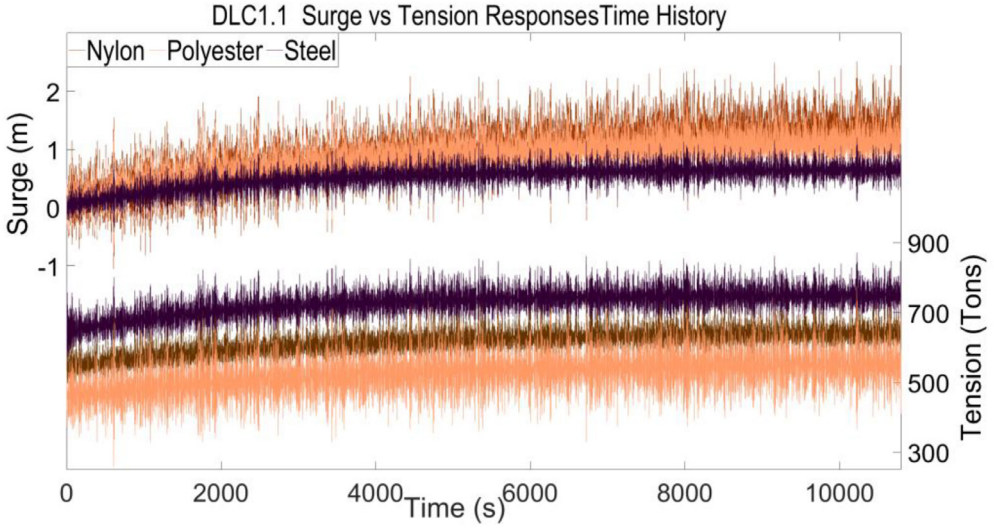

Fig. 26. Surge Response and most loaded line Tension characteristics of the TLB with Steel, Polyester, and Nylon mooring lines.

load cases. The TLB with the steel mooring line is reaching a stead mean pitch angle faster than the platform with polyester and nylon mooring lines for both DLCs. The pitching continuously increases for the TLB with the nylon mooring rope throughout the duration of the simulation due to its low stiffness. On the other hand, since steel is a very rigid material with high axial stiffness, the TLB with steel mooring lines is seen reaching the pitching equilibrium quicker. As the nylon elongates 80% more than the polyester for 20% MBF load and 100% more for 30% MBF load respectively (see Table 4). The elasticity of the nylon is the primary reason that the TLB takes longer to settle at its mean offset for pitch motion.

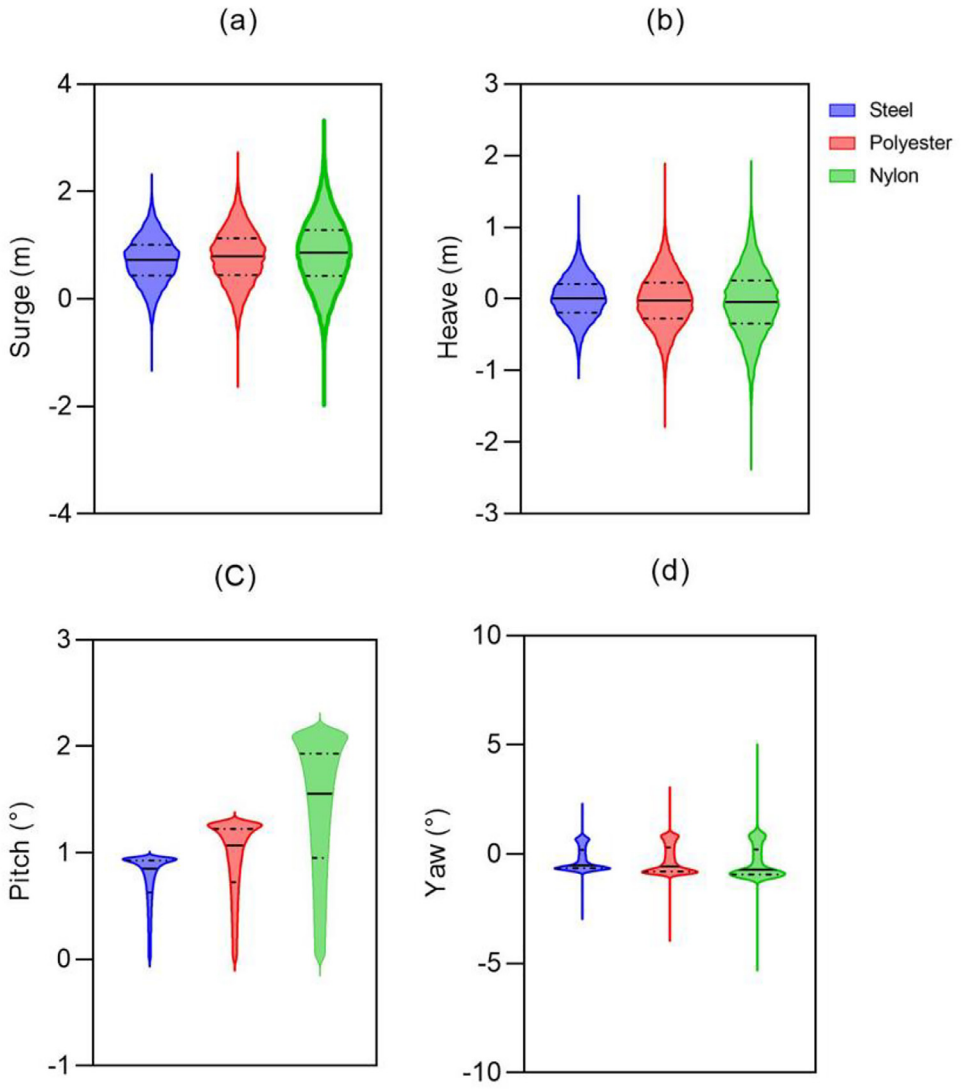

Fig. 27. Violin Plots of the Platform (a) Surge, (b) Heave, (c) Pitch, and (d) Yaw When Using Steel, Polyester, and Nylon Mooring Materials Under DLC1.6a.

Compliance with DNV regulations is investigated through the requirements given in Section 6. Using the MBL of the mooring materials showed in Table 4 that the characteristic capacity of the mooring lines, S_C for each mooring material calculated using Eq. (30). The design tension is calculated using the results for mean and maximum line tension in Table 14, Table 15, and Eq. (29) together with the ULS safety factors for normal safety class, given in Table 12. The calculations for each mooring material show in Table 16.

Comparing the results satisfy the Eq. (31) which means that all mooring lines are in compliance with DNV regulation for mooring of FOWTs. The utilization factors and safety factors calculated using Eq. (32) and (33) are show in Table 17.

$$Utilization\ Fator\ = \frac{T_d\ (N)}{S_C\ (N)} \tag{32}$$

$$Safety\ Fator = \frac{S_C\ (N)}{T_d\ (N)} \tag{33}$$

The results obtained for the TLB with three mooring materials from 3-hour environmental conditions were used to determine the maximum motion response and mooring line tension for operational conditions (DLC1.1 & DLC1.6a) are satisfied

- The rule-based limitations on response motion as set by DNVGL-RP-0286 [70]
- The design criterion for ULS as given in DNV-OS-J103 [69]

In summary, the TLB with steel mooring line has experienced smaller motion responses compared with fibre ropes and motion responses obtained from TLB with polyester are smaller compared to results from TLB with nylon mooring wire rope.

Analysis of the performance of TLB in normal and severe sea state while being operational has shown that the proposed design is capable of power production in higher sea states while allowing little motions of the nacelle and floater. Tensions are withing manufacturer described limits, the rule-based limitations, and the design criterion for ULS. The requirement to significantly alter existing control systems may even allow use of land-based systems for a TLB structure.

A critical consideration should therefore be the maximum allowable load and offset for a TLB, especially when thinking about closely spaced wind farm arrays. The results presented here show that all three turbines are operating and maintaining acceptable motion in relatively severe sea states, showing the strong advantages the TLB design has over the conventional floater and mooring types.

Table 15
TLB Motion Responses and Maximum Loaded Line (Line 8) Tension Characteristics of Steel, Polyester, and Nylon Mooring Lines for DLC1.6a.

	DLC 1.6a (NTM), V_{wind}=18 (m/s) H_s=8.8 (m) T_p=12(s)					
	Motion Response & Tension					
		Time (s)	Max	Min	Mean	Std. Dev.
Steel	**Surge(m)**	10,224	2.22	−1.23	0.72	0.43
	Heave(m)	6144	0.979	−1.03	0.01	0.30
	Pitch(deg.)	10,794	0.956	−0.01	0.74	0.25
	Yaw(deg.)	8587	1.024	−0.98	−0.24	0.52
	Tension(tons)	10,224	1089	500	831	73
Polyester	**Surge(m)**	10,224	2.60	−1.51	0.79	0.51
	Heave(m)	3433	1.38	−1.5	−0.02	0.38
	Pitch(deg.)	10,794	1.29	−0.02	0.93	0.35
	Yaw(deg.)	9475	1.24	−1.19	−0.26	0.63
	Tension(tons)	10,224	943	297	611	70
Nylon	**Surge(m)**	10,224	3.16	−1.82	0.86	0.63
	Heave(m)	6771	1.61	−2.27	−0.05	0.47
	Pitch(deg.)	10,793	2.16	−0.01	1.40	0.61
	Yaw(deg.)	10,232	1.69	−1.47	−0.38	0.71
	Tension(tons)	10,224	774	259	525	60

Table 16
Characteristic Capacity of The Mooring Lines and The Design Tension Calculations for Each Mooring Material under Operational Conditions.

		T_d (N)	
	S_C (N)	DLC1.1	DLC1.6a
Steel	2.80E+07	1.17E+07	1.50E+07
Polyester	2.70E+07	1.02E+07	1.35E+07
Nylon	2.09E+07	9.17E+06	1.10E+07

Table 17
The Utilization Factors for Each Mooring Line under Operational Conditions.

	Utilization Factor		SF	
	DLC1.1	DLC1.6a	DLC1.1	DLC1.6a
Steel	42%	54%	1.86	2.38
Polyester	38%	50%	2.00	2.65
Nylon	44%	52%	1.91	2.28

Table 18
TLB Responses Characteristics of Steel, Polyester, and Nylon Mooring Lines for DLC6.1a with Turbulence EWM and DLC6.2b with Steady EWM.

			Time (s)	Max	Min	Mean	SD
DLC6.1a	Steel	Surge(m)	6094	2.9	−2.1	0.7	0.6
		Heave(m)	6771	1.4	−1.6	0.0	0.4
		Pitch(deg.)	10,796	1.8	0.0	1.3	0.5
		Yaw(deg.)	9369	1.1	−1.6	−0.1	0.3
		Tension(tons)	6094	1448.9	355.3	908.7	147.5
	Polyester	Surge(m)	6094	3.6	−1.7	0.6	0.6
		Heave(m)	6771	1.9	−2.2	−0.1	0.5
		Pitch(deg.)	10,794	2.6	0.0	1.7	0.7
		Yaw(deg.)	6094	1.3	−2.0	−0.1	0.4
		Tension(tons)	6094	1308.5	221.2	759.5	144.6
	Nylon	Surge(m)	6094	4.6	−2.2	0.8	0.8
		Heave(m)	6771	2.2	−3.2	−0.1	0.7
		Pitch(deg.)	10,797	3.3	0.0	2.1	‘0.9
		Yaw(deg.)	8783	1.7	−2.8	−0.1	0.5
		Tension(tons)	6094	1074.2	167.9	614.9	118.1
DLC6.2b	Steel	Surge(m)	6094	2.5	−1.3	0.5	0.5
		Heave(m)	6772	1.4	−1.5	−0.1	0.4
		Pitch(deg.)	10,796	1.5	0.0	1.1	0.4
		Yaw(deg.)	9369	0.9	−1.4	0.0	0.3
		Tension(tons)	6094	1332.5	338.3	841.4	134.1
	Polyester	Surge(m)	6094	2.7	−1.5	0.6	0.6
		Heave(m)	6771	1.7	−2.0	0.0	0.5
		Pitch(deg.)	10,797	2.0	0.0	1.3	0.5
		Yaw(deg.)	5929	1.0	−1.5	−0.1	0.3
		Tension(tons)	6094	1139.7	140.2	625.1	123.4
	Nylon	Surge(m)	6094	3.3	−1.6	0.7	0.7
		Heave(m)	6771	2.2	−2.8	0.0	0.6
		Pitch(deg.)	10,796	2.4	0.0	1.5	0.7
		Yaw(deg.)	8783	1.1	−2.0	−0.1	0.3
		Tension(tons)	6094	861.7	134.7	493.2	94.8

6.2.2. Parked (Idling) event

The Parked (Idling) Event condition analysis represents a harsh sea state event under which the turbine is typically switched off. For the North Sea region, significant wave height can reach above 16 m, and an extreme wind model with high turbulence intensity representing the wind profile with 50-year return period was used. The primary objectives are to investigate first the TLB with three mooring materials will survive in such environmental conditions and second analysis the induced effect of wind turbulence intensity on motion responses of the TLB with each mooring material. Table 18 shown the summary statistics of motion responses and loaded line maximum tension for TLB with three mooring materials under parked (Idling) event. To compliance with DNV regulations the design tension is calculated using the results for mean and maximum line tension of mooring lines presented in Table 18. Fig. 28 shows the motion responses obtained under DLC6.1a and DLC6.2b, and Fig. 29 shows the percentage differences of the wind turbulence intensity effect on each mooring line. Both figures indicate that the turbulence wind model affects six-degree motion responses consequence of impact on mooring line tension. The TLB with nylon mooring rope is significantly affected due to the influence of the wind turbulence intensity, and the effect of the turbulence on the TLB with steel mooring line response is the lowest impact. The highest motion responses shown for nylon fibre rope are caused due to the elasticity of the nylon material, and the highest tension recorded for steel wire rope is due to the steel material rigidity. The polyester rope has recorded further tension than for the nylon rope. Wind turbulence has considerable effect on pitching of the TLB moored with nylon rope, indicating that line material's elasticity is crucial for the TLB motion response in turbulent wind events. The fluctuations with turbulence that cannot be seen in the simulations without turbulence specifically for the TLB with nylon mooring lines.

More specifically, the existence of the wind turbulence is seen resulting in approximately 16%, 33% and 38% increase in maximum surge motion response for steel, polyester, and nylon mooring line materials respectively; approximately 19%, 32% and 39% increase in pitch motion for steel, polyester, and nylon line materials respectively; and up to 15% in yaw motion for steel, 31% for polyester, and 39% for nylon mooring lines.

In addition, the wind model with turbulence also tends to increase maximum tension by approximately 9% in the steel mooring line, 15% in the polyester, and 25% in the nylon mooring materials.

Wind turbulence has considerable effect on pitching of the TLB moored with nylon rope (39% increase), indicating that line material's elasticity is crucial for the TLB motion response in turbulent wind events. The fluctuations with turbulence that cannot be seen in the simulations without turbulence specifically for the TLB with nylon mooring lines.

According to S_C of each mooring line which are already calculated, the design tension T_d is calculated using the results for mean and maximum line tension in Table 18 and Eq. (29) together with the ULS safety factors for normal safety class, given in Table 12. The calculations for each mooring material show in Table 19.

Comparing the results satisfy the Eq. (31) which means that all mooring lines are in compliance with DNV regulation for mooring of FOWTs. The utilization factors and safety factors are show in Table 20.

The rule-based limitations on response motion as set by DNVGL-RP-0286 [70], imply that the inclination of tilt is limited

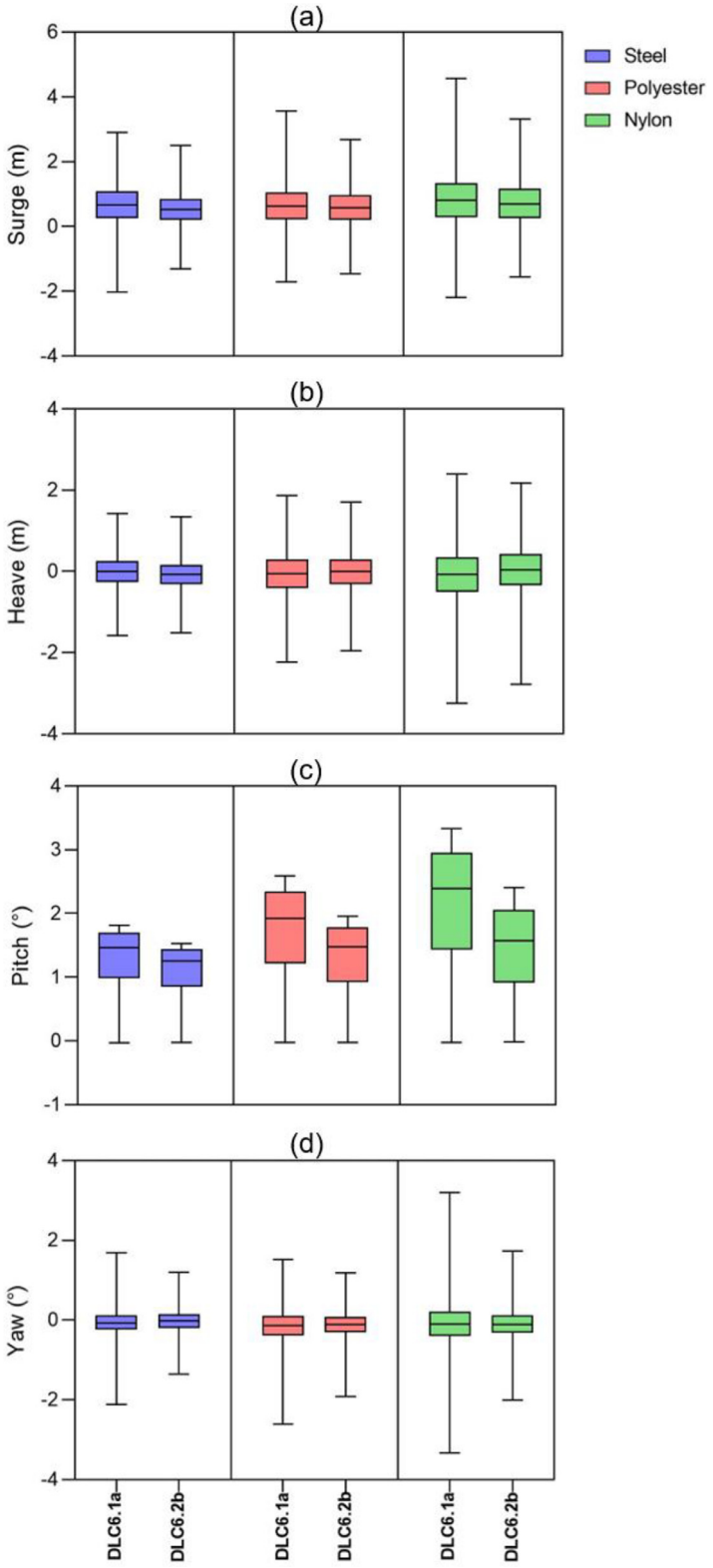

Fig. 28. Motion Responses of TLB moored with Steel, Polyester, and Nylon Mooring lines under DLC6.1a & 6.2b.

to 5° (mean value) and 10° (max. value) during operational condition and 15° (max value) for the period of non-operational condition.

The results obtained for the TLB with three mooring materials from 3-hour environmental conditions were used to determine the maximum motion response and mooring line tension for parked (Idling) event are satisfied the rule-based limitations on response motion as set by DNVGL-RP-0286 [70]. All obtained results imply that the inclination of tilt is limited to 15° (max value) for the period of non-operational condition. The mooring tensions of all three mooring materials implied with the design criterion for ULS as given in DNV-OS-J103 [69].

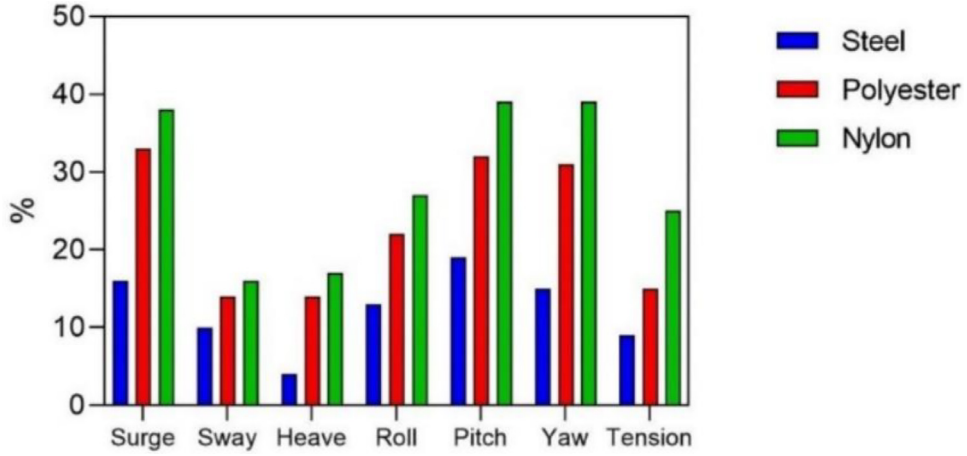

Fig. 29. Induced Effect of Wind Turbulence Intensity on Responses for TLB with Steel, Polyester, and Nylon Mooring Lines.

Table 19
Characteristic Capacity of The Mooring Lines and The Design Tension Calculations for Each Mooring Material under parked (Idling) event.

		T_d (N)	
	S_C (N)	DLC6.1a	DLC6.2b
Steel	2.80E+07	2.09E+07	1.92E+07
Polyester	2.70E+07	1.91E+07	1.68E+07
Nylon	2.09E+07	1.57E+07	1.26E+07

Table 20
The Utilization Factors for Each Mooring Line under parked (Idling) event.

	Utilization Factor		SF	
	DLC6.1a	DLC6.2b	DLC6.1a	DLC6.2b
Steel	75%	69%	1.34	1.46
Polyester	71%	62%	1.41	1.61
Nylon	75%	60%	1.33	1.66

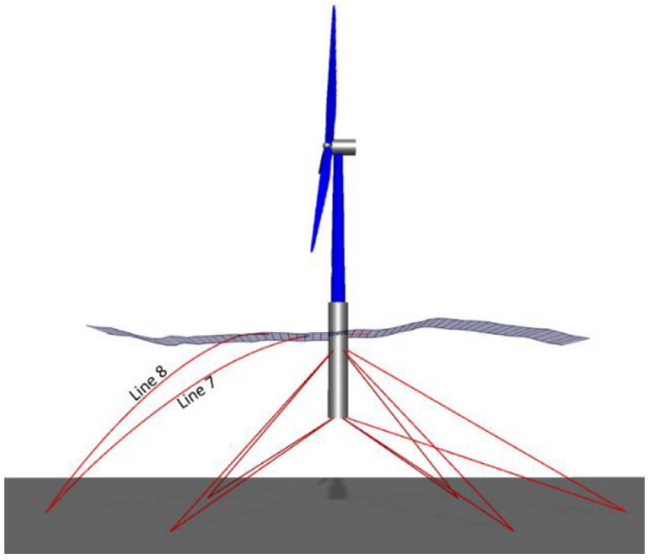

Fig. 30. Disconnected lines 7 & 8 at 100 S Representing Line Broken Scenario.

6.2.3. Parked (Idling) & fault event

As with floating offshore structures for oil and gas production, the survivability of FOWT under extreme conditions is a critical issue in design and installation. This study will now investigate the scenario of the system under broken two most loaded mooring lines in parked (idling) condition. Two most loaded lines will assume to break, and subsequently detach from the FOWT. Fig. 30 shows lines 7 & 8 are modelled to be detached from the fairlead at 100 s of the simulation for both DLCs 7.1a &7.1b. DLC7.1a. The primary objective is to investigate that the TLB with disconnected mooring lines first will survive and second the motion responses do not exceed the limitations set by DNVGL-ST-0437 [24] and DNVGL-RP-0286 [70].

Table 21 summarise the results obtained for parked (Idling) & fault events, where the tension magnitude provided is for the line which experienced the highest load. In this case, line 6 carried the maximum tension amongst the still-connected lines for both DLCs. The most striking observation for the broken line scenario is that surge and yaw motion of TLB, and dynamic tension of the most loaded mooring line, line 6, are strongly coupled following the lines has disconnected.

Figs. 31–34 show the surge, heave, yaw, and the maximum loaded line (line 6) tension for three mooring line materials under DLCs 7.1a & 7.1b. As anticipated, a significant peak in response and a robust change of frequency and amplitude in the motion responses behaviour shortly after disconnecting the mooring lines occurred. It can be noted that a sudden shift of mean offset (dotted line) after disconnecting the most loaded two lines. The sway and roll motions are small purely due to the symmetric configuration of the TLB and the incident direction of the environment. To have a clear observation for the system behaviour at the time of mooring lines broken, the first 200 s of the responses also presented in more detail. Comparing the behaviour of the three mooring materials before, during and after disconnecting the most loaded lines showed that the initial unsteady transient phase ended after the first approximately 30 s, with the system allowed to reach a steady state response before disconnecting of the lines This behaviour has been observed for all materials and is presented for the main parameters of surge, heave, yaw and the maximum dynamic tension. The sudden shift observed in motion responses after disconnections lines are higher for the TLB with nylon rope than the polyester and steel mooring lines. The platform's response with polyester and steel mooring lines is similar, with higher amplitude in the transient phase followed by separate lines from fairlead for TLB with polyester rope. The elasticity of nylon material caused higher amplitude.

The systems experienced transient phase after disconnected lines. The platform with nylon rope shown higher responses than platform with polyester and steel. For TLB with nylon a sharp high amplitude of surge and heave responses occurred in transient

Table 21
Responses Characteristics of the TLB with Steel, Polyester, and Nylon Mooring Lines for Parked (Idling) & Fault Events.

			Time (s)	Max	Min	Mean	SD
DLC7.1a	Steel	Surge(m)	611	3.91	−0.55	1.59	0.60
		Sway(m)	10,462	0.25	−1.19	−0.59	0.27
		Heave(m)	6728	2.19	0.09	1.20	0.29
		Roll(deg.)	10,667	1.17	−0.06	0.71	0.36
		Pitch(deg.)	10,800	2.47	−0.03	1.56	0.70
		Yaw(deg.)	611	2.14	1.81	1.97	0.03
		Tension(tons)	611	1637.70	416.10	1101.80	156.30
	Polyester	Surge(m)	6724	4.93	−1.12	1.96	0.73
		Sway(m)	9003	0.40	−1.45	−0.63	0.30
		Heave(m)	6731	3.05	0.13	1.62	0.39
		Roll(deg.)	10,662	1.51	−0.04	0.84	0.45
		Pitch(deg.)	10,800	2.72	−0.02	1.62	0.78
		Yaw(deg.)	6725	2.51	2.01	2.23	0.04
		Tension(tons)	6724	1448.6	429.9	922.1	136.0
	Nylon	Surge(m)	6725	5.68	−1.27	2.09	0.92
		Sway(m)	10,663	0.27	−1.71	−0.74	0.40
		Heave(m)	6729	4.17	−1.29	1.99	0.66
		Roll(deg.)	10,663	1.86	−0.05	0.90	0.55
		Pitch(deg.)	10,800	3.42	−0.01	1.86	0.98
		Yaw(deg.)	6725	2.86	2.28	2.58	0.06
		Tension(tons)	6724	1248.3	280.8	769.1	126.5
DLC7.1b	Steel	Surge(m)	6728	3.30	−0.45	1.35	0.45
		Sway(m)	6747	0.15	−0.98	−0.46	0.17
		Heave(m)	4550	1.71	0.21	0.94	0.19
		Roll(deg.)	10,771	0.98	−0.01	0.66	0.28
		Pitch(deg.)	10,793	2.13	−0.05	1.34	0.61
		Yaw(deg.)	6728	1.77	1.43	1.56	0.02
		Tension(tons)	6728	1584.4	582.9	1095.9	122.9
	Polyester	Surge(m)	6496	3.98	−0.69	1.66	0.59
		Sway(m)	6746	0.05	−1.23	−0.59	0.24
		Heave(m)	6731	2.64	0.11	1.40	0.34
		Roll(deg.)	10,758	1.31	0.00	0.80	0.38
		Pitch(deg.)	10,793	2.49	−0.03	1.48	0.71
		Yaw(deg.)	6496	2.21	1.67	1.85	0.03
		Tension(tons)	6496	1356.5	439.9	921.9	120.9
	Nylon	Surge(m)	6728	4.79	−0.86	1.69	0.72
		Sway(m)	10,663	0.19	−1.57	−0.77	0.36
		Heave(m)	6732	3.57	−0.60	1.69	0.50
		Roll(deg.)	10,662	1.70	0.00	0.92	0.49
		Pitch(deg.)	10,793	3.10	−0.02	1.69	0.89
		Yaw(deg.)	6727	2.85	2.04	2.36	0.06
		Tension(tons)	6727	1204.5	327.6	768.6	113.4

Table 22
Mean Offset Comparison of Responses under DLC7.1a & 7.1b Beforehand and Afterward Disconnected Lines.

			Average of Responses			
Mooring Material	DLC	Line Status	Surge (m)	Heave (m)	Yaw (deg.)	Tension (ton)
Steel	DLC7.1a	Before Failure	0.076	−0.085	0.048	618.68
		After Failure	1.592	1.195	1.959	1104.03
		Δ	**1.516**	**1.280**	**1.911**	**485.35**
	DLC7.1b	Before Failure	0.065	−0.022	0.080	747.89
		After Failure	1.353	0.931	1.556	1097.55
		Δ	**1.287**	**0.953**	**1.476**	**349.66**
Polyester	DLC7.1a	Before Failure	0.117	−0.056	0.151	535.13
		After Failure	1.968	1.609	2.214	923.88
		Δ	**1.851**	**1.666**	**2.063**	**388.76**
	DLC7.1b	Before Failure	0.085	−0.049	0.189	535.69
		After Failure	1.665	1.393	1.841	923.66
		Δ	**1.580**	**1.442**	**1.651**	**387.97**
Nylon	DLC7.1a	Before Failure	0.134	−0.156	0.290	464.25
		After Failure	2.096	1.975	2.564	770.46
		Δ	**1.962**	**2.130**	**2.273**	**306.21**
	DLC7.1b	Before Failure	0.096	−0.082	0.024	464.82
		After Failure	1.702	1.677	2.351	769.97
		Δ	**1.606**	**1.760**	**2.327**	**305.15**

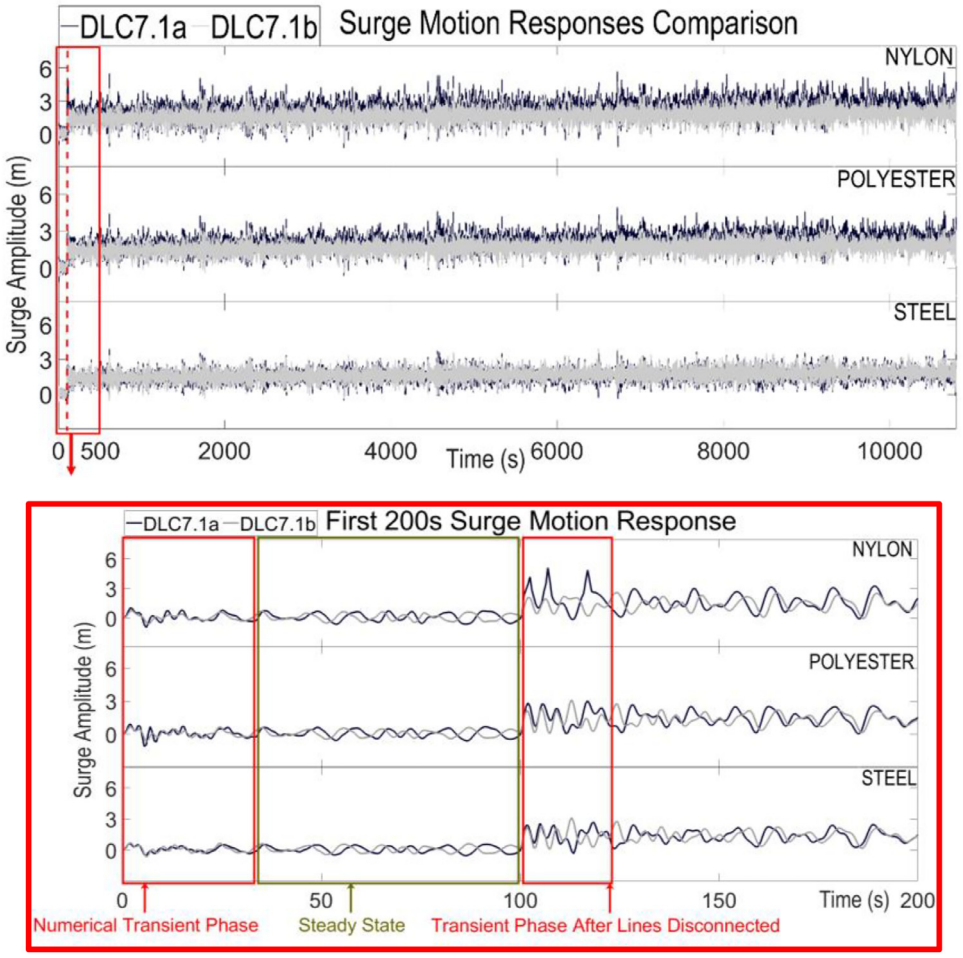

Fig. 31. DLC7.1a & 7.1b Surge Response Motion Full Time History (Top) and First 200 s (bottom) for TLB with Steel, Polyester, and Nylon Mooring Lines.

Table 23
Characteristic Capacity of The Mooring Lines and The Design Tension Calculations for Each Mooring Material under Parked (Idling) & Fault Event.

		T_d (N)	
	S_C (N)	DLC7.1a	DLC7.1b
Steel	2.80E+07	2.33E+07	2.24E+07
Polyester	2.70E+07	2.08E+07	1.92E+07
Nylon	2.09E+07	1.80E+07	1.73E+07

Table 24
The Utilization Factors for Each Mooring Line under Parked (Idling) & Fault Event.

	Utilization Factor		SF	
	DLC7.1a	DLC7.1b	DLC7.1a	DLC7.1b
Steel	83%	80%	1.20	1.25
Polyester	77%	71%	1.30	1.41
Nylon	86%	83%	1.16	1.21

phase after lines disconnected due to elasticity of the material. At 50% of the MBF, the nylon material has 31% more elasticity than the polyester. The high rigidity with higher axial stiffness for steel material caused lower magnitude. The platforms with fibre mooring lines are oscillating more after lines are disconnected.

The motion response in yaw between the three different materials shows similar response in the mean rotation before and after the lines are disconnected. The mean position in yaw after the lines are broken again is similar across all these cases. The graph shows the differences in response is strongly linked to the varying stiffness elongation characteristics between steel, nylon, and polyester. The nylon system shows significant oscillations around the mean compared to steel and polyester. In the current model, all three mooring systems are modelled to assume a delta connection, to improve the response of the nylon system the design parameters for this could be revised to be specifically designed for a less stiff system.

Surge and yaw motion responses occurred concurrently with dynamic tension for steel line materials, indicating that the surge and yaw motion are strongly coupled with the dynamic tension response of the most loaded mooring line. On the other hand, considering DLC7.1a, for fibre mooring materials, surge, heave, yaw, and dynamic tension of most loaded line occurred at same time indicating that the dynamic tension of the platform is coupled with surge, heave, and yaw motion responses. the maximum tension of the most loaded line for polyester rope is 14% and 9% higher than for nylon under DLC7.1a and DLC7.1b respectively indicating that polyester elongates less than nylon while reaching to 50% of its MBL.

The difference of mean offset before and after disconnected lines for surge, heave, and yaw motion responses, and dynamic tension of three different line materials under DLCs 7.1a & 7.1b, are shown in Table 22.

The sudden shift of mean offset for surge response after disconnecting the two lines most heavily loaded under the parked (Idling) observed, especially for the TLB moored with nylon, with a spike peak of 1.96 m and 1.61 m compared to those of steel lines,

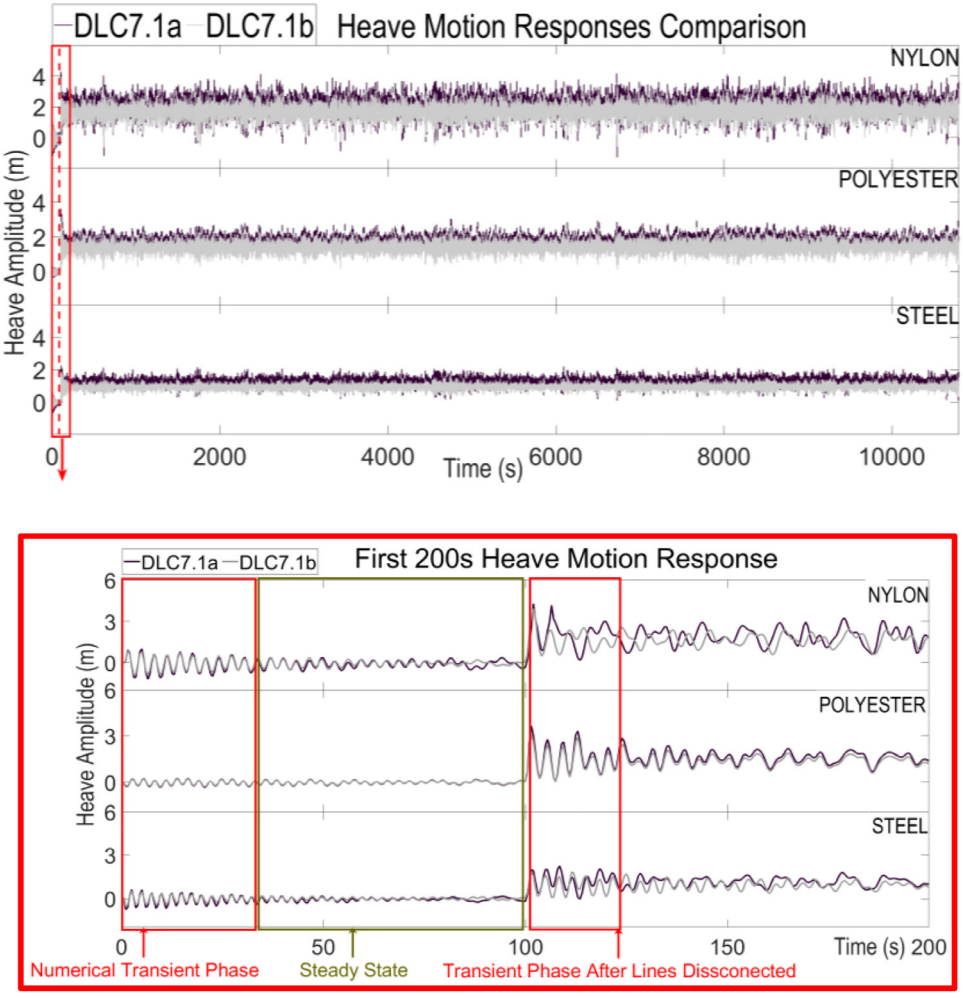

Fig. 32. DLC7.1a & 7.1b Heave Response Motion Time History for TLB with Steel, Polyester, and Nylon Mooring Lines.

1.52 m and 1.29 m, and polyester lines, 1.85 m and 1.58 m, respectively. The heave mean shift values for TLB moored with steel and polyester are smaller than with nylon. TLB with nylon experienced maximum sudden shift in heave amongst other mooring line materials with experiencing more oscillating. In terms of yaw response, the mean response of the TLB moored with nylon before lines failure raised from 0.3° to 2.6° under DLCs 7.1a and similarly from 0.02° to 2.4° under 7.1b event. amongst the three different mooring line materials, the steel mooring line recorded the highest sudden shift of mean offset under DLC7.1a ($\Delta = 485.4$ (ton)) and similarly sudden shift of mean offset of 349.7 tons under DLC7.1b.

The TLB design using three mooring lines survived in extreme sea state with wind turbulence while two loaded lines from parked events are disconnected. Base on the motion responses illustrated in Table 21, TLB with three mooring line materials satisfied the rule-based limitations on response motion as set by DNVGL-RP-0286 [70] and the design criterion for ULS as given in DNV-OS-J103 [69]. By comparing the capacity of the mooring lines and the design tension calculations (see Table 23), Table 24 shown the utilization factors for each mooring line.

6.3. Nacelle accelerations

The nacelle of the wind turbine is often undergoing cyclic movements during operations because of dynamic tower bending. These movements shall be monitored by reviewing the nacelle acceleration continuously in translational directions. According to DNVGL-RP-0286 [70] which provides guidance on limitations, the maximum nacelle acceleration should be 0.3 g (2.943 m/s^2) in the time series for the operational load cases, and should have a limit of 0.6 g (5.886 m/s^2) in the time series for the survival events.

Fig. 35 shows the maximum nacelle accelerations including translational and resultant for three mooring materials under all DLCs. By considering the absolute values present in Table 25, Fig. 36 shows the comparison of the maximum nacelle in x, y, z directions and the maximum resultant acceleration of the TLB with three mooring materials under DLCs. Fig. 36 shows the percentage of the induced effect of wind turbulence intensity on the TLB with steel, polyester, and nylon mooring lines. It observed a clear link between the maximum resultant acceleration (R) and a single motion where the resultant acceleration is higher at time steps relating to individual maximums. The resultant acceleration is the highest when x direction is the highest for three mooring materials under operational conditions. The resultant acceleration of the TLB moored with nylon is 2.45 m/s^2 under DLC1.6a which is the highest acceleration amongst other mooring materials for both operational events.

In both DLCs which are representing the parked (Idling) event condition, the TLB with nylon again has the highest nacelle resultant acceleration than the TLB moored with polyester and steel materials. The maximum resultant nacelle acceleration has a link to the maximum nacelle acceleration in z direction for all three mooring materials under DLC6.1a event. The TLB with nylon mooring line experienced the highest nacelle acceleration in x, y, and

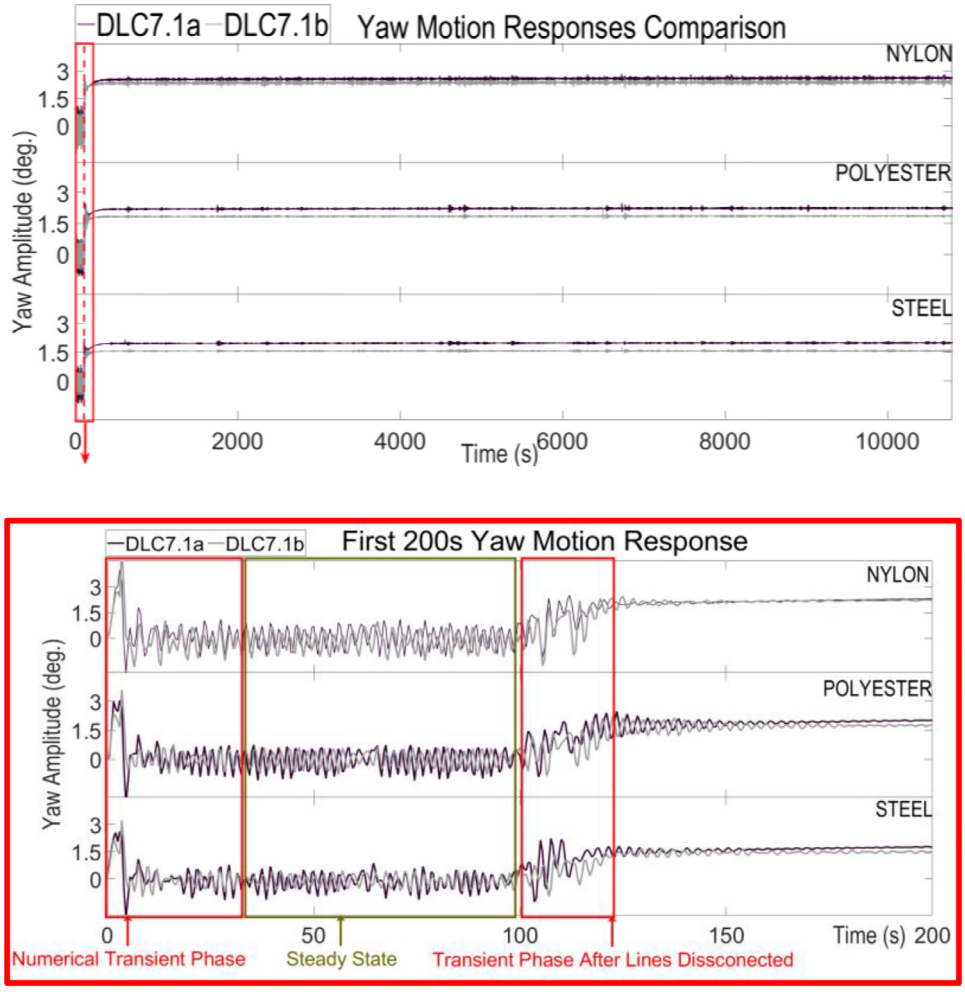

Fig. 33. DLC7.1a & 7.1b Yaw Response Motion Time History for TLB with Steel, Polyester, and Nylon Mooring Lines.

Table 25
Maximum Translational and Resultant Nacelle Acceleration.

	DLC1.1				DLC1.6a			
	X_ACC	Y_ACC	Z_ACC	R	X_ACC	Y_ACC	Z_ACC	R
Steel	−0.83	−0.09	−0.06	0.83	−1.20	0.11	0.12	1.21
Polyester	−1.08	−0.13	0.05	1.08	−1.82	−0.19	0.11	1.82
Nylon	1.26	0.05	0.15	1.26	−2.45	0.09	−0.47	2.45
	DLC6.1a				DLC6.2b			
	X_ACC	Y_ACC	Z_ACC	R	X_ACC	Y_ACC	Z_ACC	R
Steel	1.18	−1.41	1.68	1.80	1.13	−1.27	1.57	1.70
Polyester	−1.49	2.36	1.82	2.64	−1.37	2.06	1.55	2.19
Nylon	−1.94	2.71	−2.72	3.27	−1.74	2.33	−2.28	2.53
	DLC7.1a				DLC7.1b			
	X_ACC	Y_ACC	Z_ACC	R	X_ACC	Y_ACC	Z_ACC	R
Steel	−1.52	2.74	3.37	3.71	1.04	2.13	3.28	3.53
Polyester	2.03	2.97	3.63	4.11	−1.07	2.91	3.35	3.48
Nylon	2.56	3.11	4.01	4.49	2.10	2.94	3.77	4.00

z directions than the TLB with polyester and steel mooring lines. As there is an EWM with existence of turbulence in DLC6.1a, the nacelle acceleration is higher than the one for DLC6.2b. The TLB moored with nylon lines has experienced 8% and 83% more nacelle acceleration than the TLB with polyester and steel mooring lines respectively. The TLB with polyester has 69% more nacelle acceleration than the one with steel mooring line. The maximum resultant nacelle acceleration has a link to the maximum nacelle acceleration in y direction under DLC6.2b for the TLB with polyester and nylon mooring lines and has a link to the maximum nacelle acceleration in x and y direction for the TLB moored with steel mooring material. The TLB with nylon mooring lines has highest nacelle acceleration under DLC6.2b event. The TLB moored with nylon has 15% and 48% more acceleration than the TLB with polyester and steel mooring lines respectively. There is a strong link between the maximum resultant acceleration and the maximum acceleration in z direction for all mooring materials under both DLC7.1a and DLC7.1b events. As DLC 7.1a represents a harsher environmental condition than the DLC7.1b, the nacelle acceleration is higher. Similar to operational and parked events, the TLB moored with ny-

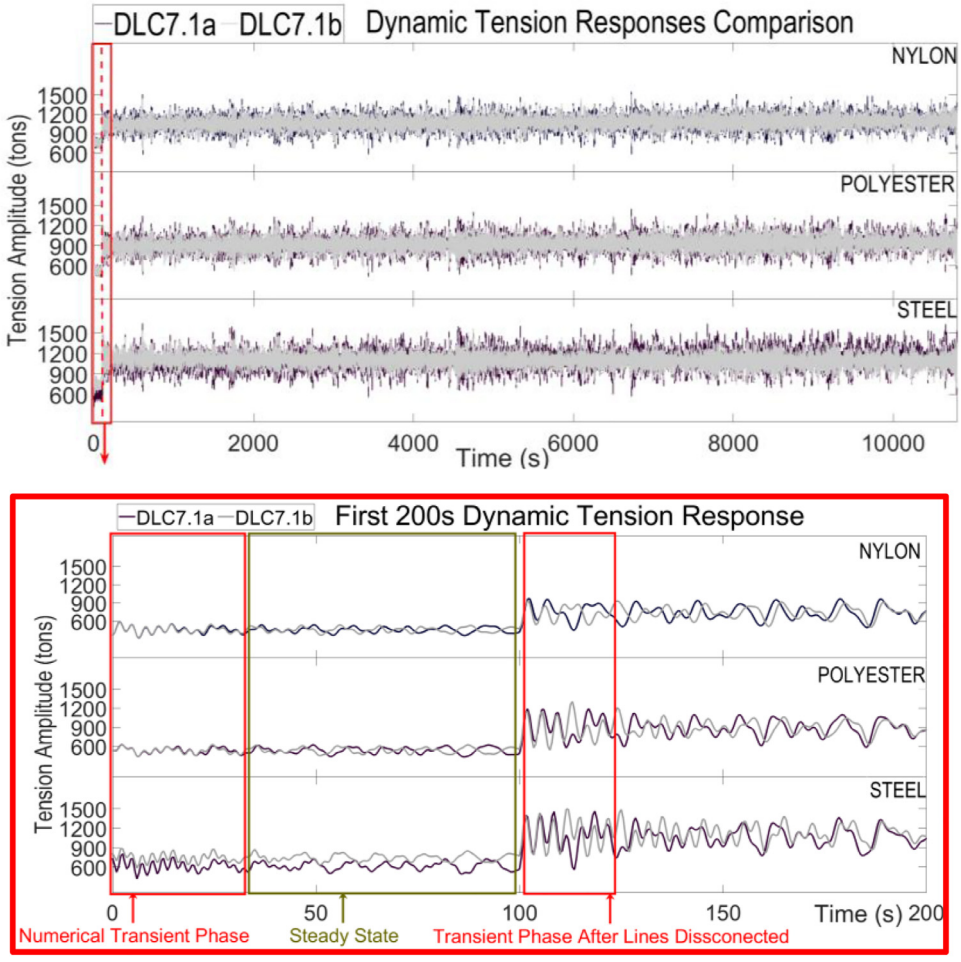

Fig. 34. DLC7.1a &7.1b Maximum Loaded Line (Line 6) Tension Load Time History for TLB with Steel, Polyester, and Nylon Mooring Lines.

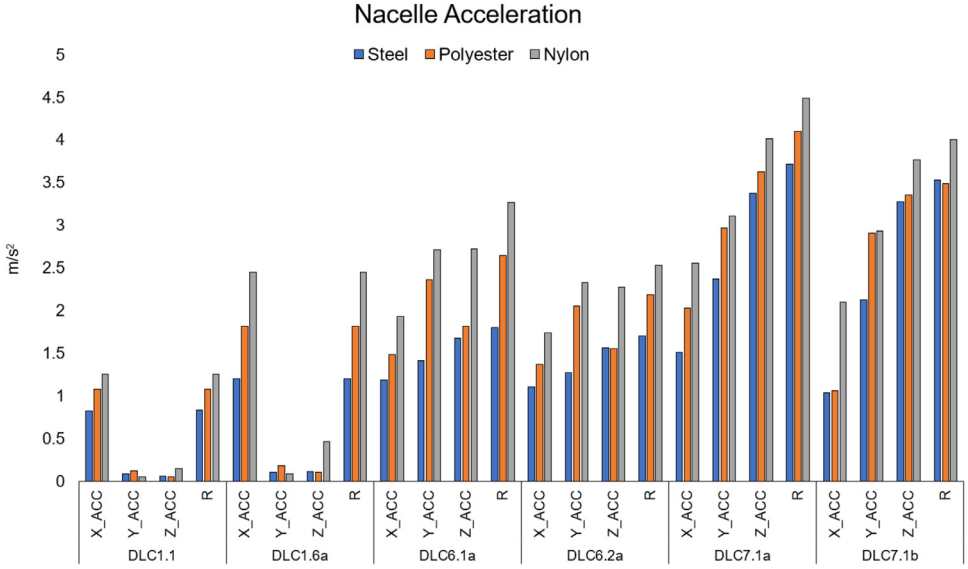

Fig. 35. TLB Moored with Polyester, Nylon, and Steel Wire Ropes Maximum Nacelle Acceleration Comparison for DLCs.

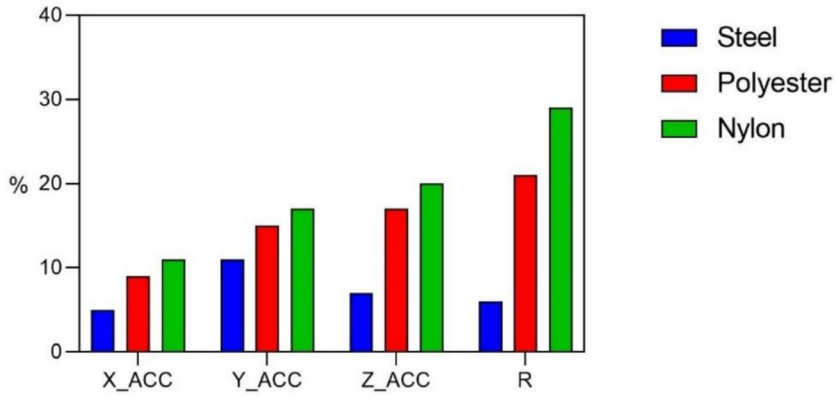

Fig. 36. Induced Effect of Wind Turbulence on Maximum Nacelle Acceleration of TLB with Steel, Polyester, and Nylon Mooring Lines.

lon experienced higher nacelle acceleration in x, y, and z directions than the TLB with polyester and steel mooring line materials under the parked with fault event.

Fig. 36 shows the induced effect of wind turbulence intensity on nacelle acceleration of the TLB with steel, polyester, and nylon mooring lines (percentage difference between DLC6.1a and DLC6.2b maximum translational accelerations). The effect of the wind turbulence on the resultant nacelle acceleration for the TLB with nylon mooring lines is higher than for the TLB moored with polyester and steel mooring lines. This is also true for nacelle acceleration in x, y, and z directions. The induced effect of wind turbulence intensity on the resultant nacelle acceleration of the TLB with steel mooring line is 6%, with polyester mooring line is 21%, and for the system moored with nylon rope is 29%.

The TLB moored with the taut mooring system of all three different line materials satisfy the DNVGL criteria for nacelle acceleration for the system in both operational (<0.3 g) and non-operational conditions (<0.6 g). It is further noted that the wind turbulence intensity and the significant wave height defined by the load cases have significant impact on the nacelle acceleration. In addition, for all load cases, it is evident that the benefits of a stiffer mooring system include the reduction of nacelle acceleration for the FOWT system.

7. Conclusions

The study demonstrates the feasibility of using a TLB FOWT system to support a wind turbine capacity of 10 MW moored by a novel taut mooring system with three different line materials available on the market. The TLB FOWT system proposed in this study is less complex, with a clear advantage in construction and installation over current leading technology FOWT types. The TLB design could be ready built in the port, ballasted and then towed out to the deployed location, and by de-ballasting, the TLB can hook into the mooring lines and achieve its design pre-tension. The expenditure on support vessels will be reduced. Therefore, the TLB design will provide a cost-effective, flexible alternative platform solution for large-scale FOWT development around the UK.

Results of the extensive time domain coupled simulations have shown that all TLB designs can operate safely in typical North Sea field conditions. Steel, Nylon and Polyester mooring lines achieve comparable motion and force responses and comply with governing regulations. The dynamic response of the floater obtained for all DLCs showed slight motion and nacelle accelerations, enabling the wind turbine to be installed without significant modifications to its control systems. Therefore, the TLB design will allow for the simplicity of adopting land-based wind turbines without needing to re-develop control systems to cope with the increased motion and accelerations. All mooring line materials considered can operate and maintain acceptable responses in relatively severe sea states producing power and can survive in extreme sea states with extreme turbulence wind model tested in the full time domain simulations.

In addition, the design was shown to survive in extreme sea states, even with the most loaded mooring lines broken and detached from the floater. More rigid mooring lines in the taut mooring system are advantageous in maintaining the TLB's stability whilst exhibiting high line tension compared to elastic mooring line materials. The taut mooring system designed for the TLB FOWT can maintain positive tension in all DLCs assessed. All three mooring lines can be utilised to moor a large-scale TLB structure due to providing a sufficient safety factor under all considered environmental conditions.

Overall, TLB designs satisfied the rule-based limitations on motion response, the design criterion for ULS and ALS and the criteria for nacelle acceleration.

Further, more detailed study should be carried out to investigate the system performance, under non-collinear environmental conditions and integrating some of the simplified modelling in terms of mooring line composition and delta connection to reduce yaw motion. A detailed cost analysis study should also be performed, to allow a precise comparison to other popular concepts for floating foundations. A laboratory experimental model test is essential (and planned) for further validation, to improve the model tools in the next stage of this study.

Declaration of Competing Interest

The authors declare that they have no known competing financial interests or personal relationships that could have appeared to influence the work reported in this paper.

References

[1] M. Beerepoot, International Energy Agency (IEA). Technology Roadmap: Solar Heating and Cooling, OECD/IEA International Energy Agency IEA Publishing, Paris, France, 2012.
[2] C. Stark, M. Thompson, C.C. Committee, Net Zero The UK's contribution to stopping global warming (2019).
[3] EWEA, Deep water (2013) 09/10/2018] Available fromhttp://www.ewea.org/fileadmin/files/library/publications/reports/Deep_Water.pdf.
[4] CATAPULT, MACROECONOMIC BENEFITS OF FLOATING OFFSHORE WIND IN THE UK (2018) 04/02/2019] Available from: 5bd78f98e76ae_Macroeconomic benefits of offshore wind in the UK -October 2018 (2).pdf.
[5] Carbon Trust, Floating Offshore Wind: Market and Technology Review (2015).
[6] A. Henderson, R. Leutz, T. Fujii, Potential for floating offshore wind energy in Japanese waters (2002).
[7] J. Zhao, L. Zhang, H. Wu, Journal of Marine Science and Application 11 (3) (2012) 328–334.
[8] D. Zwick, M. Muskulus, Wind Energy 19 (2) (2016) 265–278.

[9] Z. Shahan, History of Wind Turbines (2014) 2/3/2019]; Available fromhttps://www.renewableenergyworld.com/ugc/articles/2014/11/history-of-wind-turbines.html.
[10] CATAPULT, Floating wind: technology assessment (2015) [cited 2/2/2018; Available fromhttps://ore.catapult.org.uk/app/uploads/2018/01/Floating-wind-technology-assessment-June-2015.pdf.
[11] L. Castro-Santos, V. Diaz-Casas, Floating Offshore Wind Farms, Springer, 2016.
[12] D. Matha, et al., Phil. Trans. R. Soc. A 373 (2035) (2015) 20140350.
[13] A. Myhr, Developing offshore floating wind turbines: the Tension-Leg-Buoy design (2016).
[14] P. Sclavounos, C. Tracy, S. Lee, ASME 2008 27th International Conference on Offshore Mechanics and Arctic Engineering, American Society of Mechanical Engineers, 2008.
[15] A. Myhr, K.J. Maus, T.A. Nygaard, The Twenty-first International Offshore and Polar Engineering Conference, International Society of Offshore and Polar Engineers, 2011.
[16] J.M. Berg, Experimental and Computational Study of Tension Leg Buoy Concepts For Floating Wind Turbines, Norwegian University of Life Sciences, Ås, 2013.
[17] D.N. Veritas, Wave Analysis By Diffraction and Morison Theory (Wadam), SESAM User's Manual, Det Norske Veritas (DNV), Høvik, Norway, 1994.
[18] J. Tang, et al., OCEANS 2016-Shanghai, IEEE, 2016.
[19] MARINTEK, SIMO—User's Manual Version 3.6 (2007).
[20] D.S. Ocean, RIFLEX 4.12.2 Theory Manual (2018) Available fromhttps://home.hvl.no/ansatte/tct/FTP/H2021%20Marinteknisk%20Analyse/SESAM/SESAM%20UM%20Brukermanualer/RIFLEX%20User%20Manual.pdf.
[21] M. Lerch, et al., Sustain. Energy Technol. Assessments 30 (2018) 77–90.
[22] D.N. Veritas, DNV-OS-J101-Design of Offshore Wind Turbine Structures, Det Norske Veritas, 2004.
[23] I.E. Commission, Int. Electrotech. Commiss. (2005).
[24] DNVGL-ST-0437, 2016, Tech. rep., DNVGL.
[25] J.M. Jonkman, M.L. Buhl Jr., Wind Power Conference and Exhibition, 2007.
[26] I.E. Commission, IEC 61400-3 Wind Turbines Part3: Design Requirements For Offshore Wind Turbines, International Electrotechnical Commission, Geneva, Switzerland, 2009.
[27] G. DNV, DNVGL-OS-E301 Position Mooring, DNV GL, Oslo, 2015.
[28] G. Dnv, DNVGL-ST-0119: Floating wind Turbine Structures, DNV GL, 2018.
[29] C. Bak, et al., in: Description of the DTU 10 MW Reference Wind Turbine, DTU Vindenergi, 2013, p. 2013.
[30] J. George, Master's Thesis Project, Instituto Superior Técnico Technical University of Lisbon, Portugal, MS, 2014.
[31] J. Trolle, F. Hornbak, Department of Civil Engineering Division of Structures, Materials and Geotechnics, Aalborg University Esbjerg, Esbjerg, Denmark, 2016.
[32] X.-H. Luo, R.-C. Xiao, H.-F. Xiang, in: Cable Element Based On Exact Analytical Expressions, 33, Journal of Tongji University, 2005, p. 5.
[33] Y. Yang, J.-Y. Tsay, Int. J. Struc. Stabil. Dynam. 7 (04) (2007) 571–588.
[34] M.K. Al-Solihat, M. Nahon, Ships Offshore Struc. 11 (8) (2016) 890–904.
[35] BRINDON.BEKAERT, MoorLine Polyester (2018) 7/9/2019]; Available fromhttps://www.bridon-bekaert.com/en-gb/steel-and-synthetic-ropes/offshore-production/mooring.
[36] I. Ćatipović, V. Čorić, J. Radanović, in: An Improved Stiffness Model For Polyester Mooring Lines, 62, Teorija i praksa brodogradnje i pomorske tehnike, Brodogradnja, 2011, pp. 235–248.
[37] A. Rp, Design and Analysis of Stationkeeping Systems For Floating Structures, American Petroleum Institute, 2005.
[38] D.N. Veritas, G. Lloyd, Recommended Practice For design, Testing and Analysis of Offshore Fibre Ropes (DNVGL-RP-E305), DNVGL Press, 2017.
[39] ABS, THE APPLICATION OF FIBER ROPE FOR OFFSHORE MOORING (2014) 2/8/2019]; Available fromhttps://ww2.eagle.org/content/dam/eagle/rules-and-guides/current/offshore/90_fiberrope/fiber_rope_gn_e-feb14.pdf.
[40] E. Falkenberg, V. Åhjem, L. Yang, Offshore Technology Conference, OnePetro, 2017.
[41] E. Falkenberg, L. Yang, V. Åhjem, International Conference on Offshore Mechanics and Arctic Engineering, American Society of Mechanical Engineers, 2018.
[42] M. Francois, et al., Offshore Technology Conference, OnePetro, 2010.
[43] H. Liu, et al., An experimental investigation on nonlinear behaviors of synthetic fiber ropes for deepwater moorings under cyclic loading, Applied Ocean Research 45 (2014) 22–32.
[44] A. Fernandes, C. Del Vecchio, G. Castro, Mechanical properties of polyester mooring cables, International Journal of Offshore and Polar Engineering 9 (03) (1999).
[45] M.B. Huntley, OCEANS 2016 MTS/IEEE Monterey, IEEE, 2016.
[46] K.-T. Ma, et al., Mooring System Engineering For Offshore Structures, Gulf Professional Publishing, 2019.
[47] M. Francois, P. Davies, Fibre rope deep water mooring: a practical model for the analysis of polyester mooring systems, in: Proceedings of Oil Gas Conference, Rio de Janeiro, 2000.
[48] C. Chaplin, C. Del Vecchio, Offshore Technology Conference, Offshore Technology Conference, 1992.
[49] D.N. Veritas, WADAM—Wave Analysis by Diffraction and Morison Theory, SESAM user's manual, Høvik, 1994.
[50] C.-H. Lee, J. Newman, WIT Transac. State Art Sci. Engin. (2005) 18.
[51] A. Jiawen Li, B.Yougang Tang, C.R.W. Yeung, J. Renew. Sustain. Energy 6 (3) (2014) 033102.
[52] Q. Cao, et al., Renew. Energy (2020).
[53] M.I. Kvittem, T. Moan, J. Offshore Mechan. Arctic Engineering 137 (1) (2015) 011901.
[54] C. Luan, Z. Gao, T. Moan, Marine Struc. 51 (2017) 87–109.
[55] M. Karimirad, T. Moan, Marine Struc. 27 (1) (2012) 45–63.
[56] C. Luan, et al., Energy Procedia 137 (2017) 366–381.
[57] B. Jonkman, L. Kilcher, TurbSim User's guide: Version 1.06. 00, National Renewable Energy Laboratory, Golden, CO, USA, 2012.
[58] S.N. Godø, Trondheim, 2013, Norwegian University of Science and Technology, 2013.
[59] C. Lee, Theory Manual (1995).
[60] O. Faltinsen, Sea Loads On Ships and Offshore Structures, 1, Cambridge university press, 1993.
[61] K.O. Ronold, et al., International Conference on Offshore Mechanics and Arctic Engineering, 2010.
[62] Z. Chuang, S. Liu, Y. Lu, Int. J. Naval Architec. Ocean Engineering 12 (2020) 367–375.
[63] H. Lee, S.K. Poguluri, Y.H. Bae, Energies 11 (2) (2018) 406.
[64] S. Liu, A. Papanikolaou, G. Zaraphonitis, ICMT conference, 2014.
[65] G.K.Y. Chan, et al., International Conference on Offshore Mechanics and Arctic Engineering, American Society of Mechanical Engineers, 2015.
[66] D.N. Veritas, Recommended Practice DNV-RP-C205: Environmental Conditions and Environmental Loads, DNV, Norway, 2010.
[67] I. Langen, R. Sigbjörnsson, Dynamisk Analyse Av konstruksjoner: Dynamic analysis of Structures, Tapir, 1979.
[68] C. Larsen, Marine dynamics: TMR4182 Marine dynamics, Akademika forlag Kompendieforlaget, Trondheim, 2014.
[69] D.N. Veritas, DNV-OS-J103: Design of Floating Wind Turbine Structures, DNV, DNV, Nor-way, 2013.
[70] DNV, G., *Recommended Practice: coupled analysis of floating wind turbines*. 2019, DNVGL-RP-0286. DNV GL AS, Høvik, Oslo, Norway.